



Review

Hyperspectral remote sensing of fire: State-of-the-art and future perspectives

Sander Veraverbeke^{a,*}, Philip Dennison^b, Ioannis Gitas^c, Glynn Hulley^d, Olga Kalashnikova^d, Thomas Katagis^c, Le Kuai^{d,e}, Ran Meng^f, Dar Roberts^g, Natasha Stavros^d

^a Vrije Universiteit Amsterdam, De Boelelaan 1085, 1081 HV Amsterdam, the Netherlands

^b University of Utah, 332 S 1400 E, 84112 Salt Lake City, USA

^c University of Thessaloniki, 59 Mouschounti Street, 55134 Thessaloniki, Greece

^d NASA Jet Propulsion Laboratory, California Institute of Technology, 4800 Oak Grove Drive, 91109 Pasadena, USA

^e University of California, Los Angeles, USA

^f Brookhaven National Laboratory, P.O. Box 5000, 11973 Upton, USA

^g University of California, Santa Barbara, 5832 Ellison Hall, 93106 Santa Barbara, USA



ARTICLE INFO

Keywords:

Hyperspectral
Imaging spectroscopy
Fire
Fuel
Fire severity
HyspIRI
AVIRIS

ABSTRACT

Fire is a widespread Earth system process with important carbon and climate feedbacks. Multispectral remote sensing has enabled mapping of global spatiotemporal patterns of fire and fire effects, which has significantly improved our understanding of interactions between ecosystems, climate, humans and fire. With several upcoming spaceborne hyperspectral missions like the Environmental Mapping And Analysis Program (EnMAP), the Hyperspectral Infrared Imager (HyspIRI) and the Precursore Iperspettrale Della Missione Applicativa (PRISMA), we provide a review of the state-of-the-art and perspectives of hyperspectral remote sensing of fire. Hyperspectral remote sensing leverages information in many (often more than 100) narrow (smaller than 20 nm) spectrally contiguous bands, in contrast to multispectral remote sensing of few (up to 15) non-contiguous wider (greater than 20 nm) bands.

To date, hyperspectral fire applications have primarily used airborne data in the visible to short-wave infrared region (VSWIR, 0.4 to 2.5 μm). This has resulted in detailed and accurate discrimination and quantification of fuel types and condition, fire temperatures and emissions, fire severity and vegetation recovery. Many of these applications use processing techniques that take advantage of the high spectral resolution and dimensionality such as advanced spectral mixture analysis. So far, hyperspectral VSWIR fire applications are based on a limited number of airborne acquisitions, yet techniques will approach maturity for larger scale application when spaceborne imagery becomes available. Recent innovations in airborne hyperspectral thermal (8 to 12 μm) remote sensing show potential to improve retrievals of temperature and emissions from active fires, yet these applications need more investigation over more fires to verify consistency over space and time, and overcome sensor saturation issues. Furthermore, hyperspectral information and structural data from, for example, light detection and ranging (LiDAR) sensors are highly complementary. Their combined use has demonstrated advantages for fuel mapping, yet its potential for post-fire severity and combustion retrievals remains largely unexplored.

1. Introduction

Fire is a ubiquitous disturbance agent in the terrestrial biosphere and fire occurs in ecosystems that range from tropical rainforest to deserts and boreal forests (Bond and Keeley, 2005; Bowman et al., 2009). Fire occurs in a variety of forms including high intensity crown fires to long-duration ground fires in organic soils with relatively low intensity (van der Werf et al., 2017). Ecosystems and fire regimes are

rapidly changing at historically unprecedented rates (Dennison et al., 2014; Gillett et al., 2004; Stavros et al., 2014; Westerling, 2006). For example, fire activity has significantly increased in boreal forest ecosystems (Gillett et al., 2004; Turetsky et al., 2011; Veraverbeke et al., 2017) and declined in savannas (Andela et al., 2017; Andela and van der Werf, 2014).

The fire disturbance continuum discriminates between discrete temporal phases during which fire processes occur (Jain et al., 2004).

* Corresponding author.

E-mail addresses: s.s.n.veraverbeke@vu.nl (S. Veraverbeke), dennison@geog.utah.edu (P. Dennison), igitas@for.auth.gr (I. Gitas), Glynn.Hulley@jpl.nasa.gov (G. Hulley), Olga.Kalashnikova@jpl.nasa.gov (O. Kalashnikova), thkatag@for.auth.gr (T. Katagis), Le.Kuai@jpl.nasa.gov (L. Kuai), ranmeng@bnl.gov (R. Meng), dar@geog.ucsb.edu (D. Roberts), Natasha.Stavros@jpl.nasa.gov (N. Stavros).

<https://doi.org/10.1016/j.rse.2018.06.020>

Received 22 November 2017; Received in revised form 23 May 2018; Accepted 16 June 2018
0034-4257/ © 2018 Elsevier Inc. All rights reserved.



Fig. 1. Temporal phases in the fire disturbance continuum (after Jain et al., 2004).

The fire disturbance continuum includes pre-fire, active, and post-fire environments (Fig. 1). The pre-fire environment refers to the type, and condition of fuels as influenced by climate, weather and land management. The active fire environment is the phase during which fires spread over the landscape. Topography, fuels and fire weather influence active fire behavior and intensity. Fire intensity describes the physical combustion process of energy release from organic matter (Keeley, 2009) and is directly related to fire emissions (Wooster et al., 2005). Finally, the post-fire environment is what is left after the fire is extinguished. The post-fire environment is often described interchangeably with the terms fire and burn severity (Boer et al., 2008; Keeley, 2009). Here, we define fire severity as the degree of environmental change caused by a fire as evidenced immediately after the fire without recovery effects (Lentile et al., 2006; Morgan et al., 2014; Veraverbeke et al., 2010). Conversely, burn severity gauges both the immediate fire-induced change and vegetation recovery. Fire and burn severity include fire effects on vegetation and soil (Key and Benson, 2006; Morgan et al., 2014; Parsons et al., 2010).

Remote sensing has been successfully applied in all stages of the fire disturbance continuum for several decades. Success stories include fuel type mapping (Marino et al., 2016; Mitri and Gitas, 2006; Peterson et al., 2013; Roberts et al., 2003), fire risk assessments (Chuvieco et al., 2004; Meng et al., 2017; Yu et al., 2017), active fire detection (Giglio et al., 2003; Schroeder et al., 2014), burned area mapping (Barbosa et al., 1999; Giglio et al., 2009; Gitas et al., 2008; Katagis et al., 2014; Koutsias and Karteris, 2000; Pereira, 2003; Roy et al., 2005), fire/burn severity assessments (Eidenshink et al., 2007; Meng et al., 2017; Veraverbeke et al., 2010), and vegetation recovery mapping (Lewis et al., 2017; Riaño et al., 2002; van Leeuwen et al., 2010; Veraverbeke et al., 2012a). These applications have primarily capitalized upon broadband multispectral remote sensing data. Broadband multispectral remote sensing is the simultaneous acquisition of calibrated radiance units in a limited number (generally in the order between three and 15) of non-contiguous broad (generally wider than 20 nm) spectral bands. In contrast, narrowband hyperspectral remote sensing is the simultaneous acquisition of calibrated radiance in many (generally more than 100) narrow (generally 20 nm or smaller) spectrally contiguous bands. Hyperspectral imaging, or imaging spectroscopy, refers to the acquisition of coregistered images over contiguous narrow spectral bands (Schaeppman et al., 2009). Hyperspectral remote sensing has proven its utility in a wide range of Earth system science domains including fire applications (e.g. Dennison and Roberts, 2009; Schepers et al., 2014; Veraverbeke et al., 2014). Prior hyperspectral fire studies were mostly conducted based on airborne imagery, often from the Airborne Visible/Infrared Imaging Spectrometer (AVIRIS, Green et al., 1998), or the Airborne Prism Experiment (APEX, Itten et al., 2008). To date, Hyperion on the Earth-Observing One (EO-1) platform acquiring data between 2000 and 2017 has been the only spaceborne hyperspectral imager that acquired data in the visible to short-wave infrared spectral range (approximately between 0.4 and 2.5 μm) (Pearlman et al., 2003). In the next few years several spaceborne hyperspectral sensors may be launched: Environmental Mapping And Analysis Program (EnMAP, Stuffer et al., 2007), Hyperspectral Imager Suite (HISUI, Iwasaki et al., 2011), Hyperspectral Infrared Imager (HyspIRI, Lee et al., 2015), Precursore Iperspettrale Della Missione Applicativa (PRISMA, Labate et al., 2009), and the Space-borne Hyperspectral Applicative Land and Ocean

Mission (SHALOM, Feingersh and Ben Dor, 2016). These missions will greatly increase the availability and application of hyperspectral data. Furthermore, a global hyperspectral mapping mission was recently recommended by the Decadal Survey for Earth Science and Applications from Space from the National Academy of Sciences from the USA (National Academies of Sciences, 2018).

With upcoming spaceborne hyperspectral missions and the proven utility of hyperspectral data in fire applications, we provide a review of the current state-of-the-art in hyperspectral remote sensing of fire. We therefore review developments in the pre-fire, active fire, and post-fire stages of the fire disturbance continuum. Benefits from hyperspectral retrievals may result from the characterization of narrow spectral features (e.g. water or gaseous absorption, Kuai et al. (2016), Yebra et al. (2013)) because of the high spectral resolution and/or detailed spectral signatures because of higher spectral data dimensionality (Veraverbeke et al., 2014).

The primary focus of this review is on applications where hyperspectral data provides a clear improvement over multispectral data, or on novel opportunities that arise from hyperspectral data that are not possible based on multispectral data. We also propose avenues for further research.

2. Hyperspectral fire applications

2.1. Pre-fire applications

The pre-fire environment refers to fuel type and condition (Chuvieco et al., 2003a, 2003b) and how these change through time as a function of climate, weather, land management, and land use. First, fuel type represents an association of fuel elements of vegetation species, form, size arrangement and continuity that results in a characteristic fire behavior (Merrill and Alexander, 1987). Fuel type affects the chemical composition and thus available energy content that then affects fire intensity, the physical combustion process of energy release from organic matter (Agee, 1993; Keeley, 2009). Second, fuel condition refers to the moisture content and the live or dead fuel status. These parameters influence fuel drying and combustion (Pickett et al., 2010). Moisture content affects the flammability of fuels and thus fire behavior such as ignition probability and fire spread rate and consequent smoke impacts (Anderson, 1970; Forkel et al., 2012).

Multispectral remote sensing of fuel type by mapping plant functional types has capitalized upon classification and vegetation index approaches (Bartholomé and Belward, 2005; Friedl et al., 2002; Hansen and Reed, 2000; Loveland et al., 2000; Nelson et al., 2013; Rollins et al., 2006; Ryan and Opperman, 2013). Similarly, retrieving fuel moisture and photosynthetic, i.e. live, versus non-photosynthetic, i.e. dead, vegetation from multispectral data is often based on spectral indices (Anderson et al., 2004; Gao, 1995; Jackson et al., 2004; Liu and Kogan, 1996); sometimes augmented with land surface temperature data from thermal bands (Chuvieco et al., 2003a, 2003b; Verbesselt et al., 2002). Empirical relationships between spectral indices and fuel moisture are regionally specific (Jurdao et al., 2013; Riano et al., 2005; Yebra et al., 2013). Physically based radiative transfer models (RTMs) have been used to overcome site-specificity of empirical fuel moisture estimation methods (Yebra et al., 2013). These models estimate fuel moisture content as the ratio between equivalent water thickness and dry matter

Table 1
Summary of hyperspectral fire studies in pre-fire, active and post-fire environments. Fuel condition refers to dead or live fuel status, and moisture condition. (radiative transfer model: RTM, SF: spectral fitting, SI: spectral index, SMA: spectral mixture analysis).

	Reference	Application	Methods	
Pre-fire	Ustin et al. (1998)	Fuel condition	RTM, SF and SMA	
	Serrano et al. (2000)	Fuel condition	SI	
	Dennison et al. (2003)	Fuel condition	SF	
	Roberts et al. (2003)	Fuel type and condition	SI and SMA	
	Roberts et al. (2006)	Fuel type and condition	SI and SMA	
	De Santis et al. (2006)	Fuel condition	SI	
	Jia et al. (2006a)	Fuel condition	SMA	
	Jia et al. (2006b)	Fuel type and condition	SMA	
	Varga and Asner (2008)	Fuel condition	SMA	
	Al-Moustafa et al. (2012)	Fuel condition	SI	
	Colgan et al. (2012)	Fuel type	Classification	
	Casas et al. (2014)	Fuel condition	RTM, SF and SI	
	Levick et al. (2015)	Fuel type	Classification	
	Stavros et al. (2018)	Fuel type	SMA	
Active fire	Vodacek et al. (2002)	Fire detection	Potassium emission line	
	Dennison (2006)	Fire detection	SI	
	Dennison et al. (2006)	Fire temperature	SMA	
	Dennison and Roberts (2009)	Fire detection	SI	
	Amici et al. (2011)	Fire detection	Potassium emission line	
	Dennison and Matheson (2011)	Fire detection and temperature	SI and SMA	
	Matheson and Dennison (2012)	Fire detection and temperature	SI and SMA	
	Post-fire	Qiu et al. (1998)	Recovery	SI
		Riaño et al. (2002)	Recovery	SI and SMA
		van Wagtenonk et al. (2004)	Severity	SI
		Chuvieco et al. (2006)	Severity	SI and RTM
		Jia et al. (2006b)	Severity	Classification
		Kokaly et al. (2007)	Severity	Classification
		Lewis et al. (2007)	Severity	SMA
Robichaud et al. (2007)		Severity	SMA	
Lewis et al. (2008)		Severity	SMA	
Mitri and Gitas (2010)		Recovery	Classification	
Lewis et al. (2011)		Severity	SMA	
Numata et al. (2011)		Recovery	SI	
Huesca et al. (2013)		Severity and recovery	SI and SMA	
Mitri and Gitas (2013)		Recovery	Classification	
Schepers et al. (2014)	Severity	SI		
Veraverbeke et al. (2014)	Severity	SMA		
Somers et al. (2016)	Severity and recovery	SI and SMA		
Chen (2017)	Severity	SI and SMA		
Lewis et al. (2017)	Severity	SMA		
Meng et al. (2018)	Recovery	Classification		
Tane et al. (2018)	Severity	SMA		

content, which are two common parameters in RTMs (Jurdao et al., 2013). Robust and useful applications of multispectral pre-fire remote sensing are abundant. The fact that reflectance data from a few bands, often combined in a spectral index, results in high correlations with multiple fuel attributes, however, demonstrates that some of these attributes are highly correlated, yet broadband remote sensing may not be able to fully capture subtle differences that may exist between fuel type and condition.

The multiple and narrow spectral bands from hyperspectral remote sensing allow different approaches to determine fuel type and condition

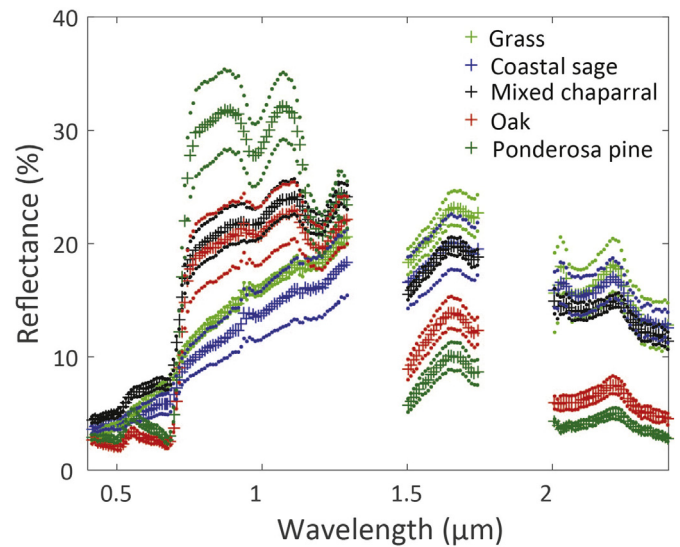


Fig. 2. Example of fuel type spectral library. The mean (symbol in plot: +) and the mean plus/minus one standard deviation (symbol in plot: .) of five spectra per vegetation type is plotted. Atmospheric water vapor absorption regions were removed.

(Schimel et al., 2013; Thompson et al., 2017). Fuel type and fractional cover can be determined from spectral mixture analysis (SMA) (Jia et al., 2006a, 2006b; Roberts et al., 2006; Roberts et al., 2003; Stavros et al., 2018) (Table 1). SMA calculates cover fractions of different ground cover classes and thereby leverages the spectral information over multiple wavebands (Adams et al., 1986; Roberts et al., 1998). Because there is inherent variability within a ground cover class, often many sample spectra, or endmembers, can be used for a single class. Multiple endmember SMA (MESMA) is an extension of SMA that accounts for variability within endmember classes (Roberts et al., 1998; Rogge et al., 2006), which is beneficial for cover fraction retrievals. For fuel type mapping, the ground cover classes can be as specific as ecosystem type and contain multiple slightly variable spectra (Fig. 2). Ground cover classes can also be defined as green vegetation (GV), non-photosynthetic vegetation (NPV), and substrate (Roberts et al., 1998). The spatial distribution of GV, NPV and substrates in a Californian landscape is shown in Fig. 3. NPV is highly flammable and its fractional cover has been used as a fire risk indicator (Jia et al., 2006a; Roberts et al., 2006; Varga and Asner, 2008). Fuel moisture content can be derived from hyperspectral signals in spectral regions with high water absorption (Ustin et al., 1998; Yebra et al., 2013). Broad spectral changes due to changes in fuel moisture content include a decrease in near infrared (NIR) and increase in short-wave infrared (SWIR) (Fig. 4). Narrow spectral changes include decreases in the depth of the absorption by liquid water centered on approximately 0.97, 1.20, 1.45, 1.94 and 2.50 μm (Fig. 4) (Tucker, 1980; Yebra et al., 2013). Studies utilizing hyperspectral data have capitalized upon these narrow spectral features by using spectral indices that input one or multiple narrowbands centered around a water absorption feature or the first derivative of the reflectance spectra (Al-Moustafa et al., 2012; Cao and Wang, 2017; Casas et al., 2014; De Santis et al., 2006; Roberts et al., 2006; Schlerf et al., 2005; Serrano et al., 2000). Approaches taking advantage of contiguous spectral information have included spectral fitting of water absorption features (Casas et al., 2014; Dennison et al., 2003; Serrano et al., 2000) and RTMs (Casas et al., 2014). Schlerf et al. (2005) and Roberts et al. (2006) reported higher accuracies from airborne hyperspectral retrievals compared to spaceborne multispectral retrievals. Cheng et al. (2006) furthermore retrieved equivalent water thickness based on applying a RTM on AVIRIS data.

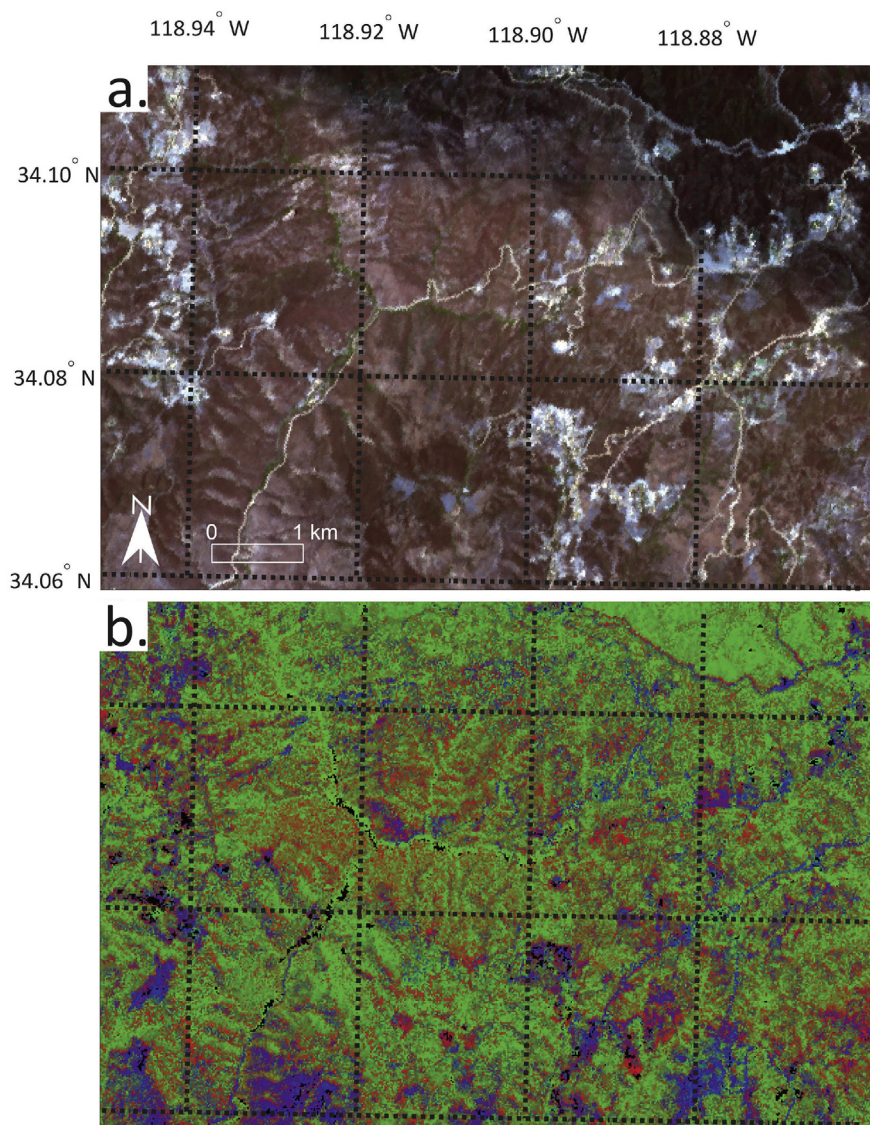


Fig. 3. a) True color composite from the Airborne Visible/Infrared Imaging Spectrometer over parts of the Santa Monica mountains in California, USA on June 16, 2016. The composite used the bands centered at 0.65 μm (red), 0.55 μm (green) and 0.45 μm (blue). b) False color composite inputting non-photosynthetic vegetation (NPV, red), green vegetation (green) and substrate (blue) cover fractions retrieved from multiple endmember spectral mixture analysis. Suboptimal retrievals were masked in black. NPV is highly flammable and its fractional cover is thus a useful fire risk indicator. (For interpretation of the references to color in this figure legend, the reader is referred to the web version of this article.)

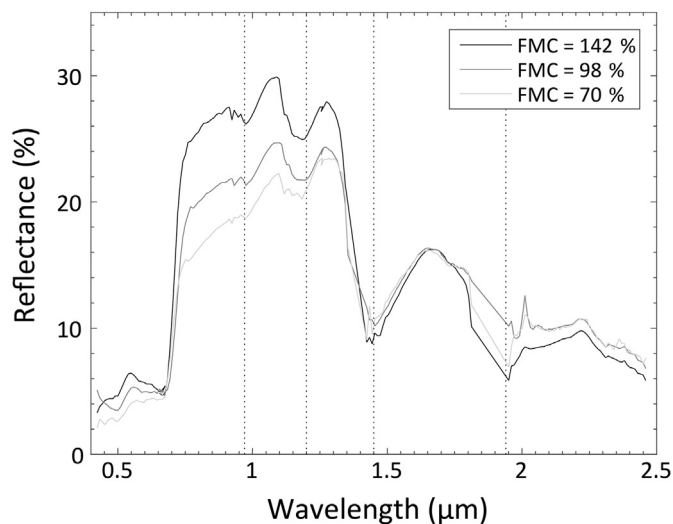


Fig. 4. Chamise spectra with fuel moisture content of 70, 98 and 142% measured in Southern California, USA. The vertical dotted lines denote key liquid water absorption features (after Roberts et al., 2006).

2.2. Active fire applications

Applications developed for active fires fall into two major categories: 1) fire detection, in which the goal is to identify spectra containing active fire (Dennison and Roberts, 2009), and 2) fire temperature retrieval, in which the goal is to model fire temperature from emitted radiance (Dennison et al., 2006). Fire temperature retrieval may provide additional outputs from modeling, such as sub-pixel fire fractional area.

Radiance emitted directly from a fire is dependent on the temperature and emissivity of the burning biomass and flame, and the flame length and depth. Traditional broadband methods for detecting fire, estimating fire temperature and intensity use brightness temperature, which assumes that fire is a blackbody emitter (Giglio et al., 2003; Roberts and Wooster, 2008; Schroeder et al., 2014; Zhukov et al., 2006). For a blackbody, emitted radiance increases and peak emission shifts to shorter wavelengths as fire temperature increases (Fig. 5).

Background blackbody surfaces at typical Earth surface temperatures emit most of their radiance in the thermal infrared (TIR: 8–12 μm) and longer wavelengths (Fig. 5). As temperature increases above 600 K, radiance in the mid infrared (MIR: 3–5 μm) and SWIR (1.2–2.5 μm) sharply increases. Smoke is a strong scatterer and absorber at wavelengths shorter than 1.2 μm , such that the visible (0.4–0.7 μm) and NIR

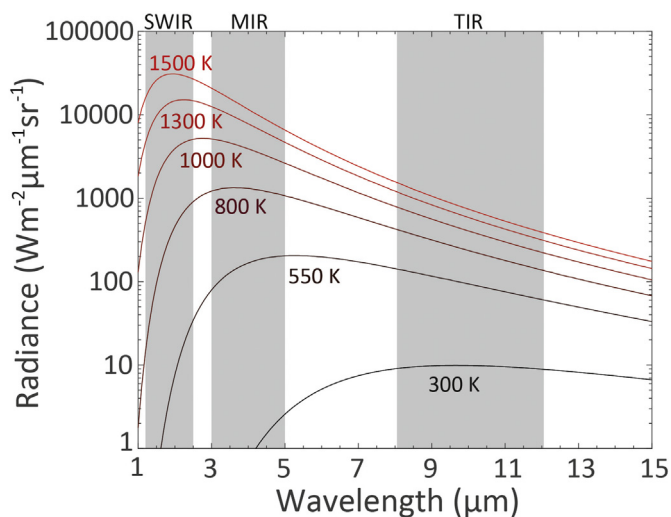


Fig. 5. Blackbody emission curves across a range of temperatures (after Dennison and Matheson, 2011). Grey areas denote the short-wave infrared (SWIR), mid infrared (MIR) and thermal infrared (TIR) spectral regions.

(0.7–1.2 μm) spectral regions have limited utility for active fire applications. At longer wavelengths, smoke transmittance is very high and smoke has a very minor impact on emitted radiance. Thus, the SWIR and MIR spectral regions are most useful for measuring flaming and smoldering combustion (Dennison and Matheson, 2011). The SWIR spectral region demonstrates a very strong difference in emitted spectral radiance across the range of temperatures typical for smoldering and flaming combustion (650 K to higher than 1500 K).

While multiple active fire applications of hyperspectral data have assumed that fire within an instantaneous field of view (i.e. a pixel) is a single temperature blackbody (Dennison et al., 2006; Dennison and Matheson, 2011; Matheson and Dennison, 2012), the actual shape of emitted radiance is a critically important question. Emitted radiance from a single pixel will be a composite of multiple flaming and smoldering elements, each with their own range of temperatures. At-sensor radiance itself will be a combination of burning and non-burning surfaces within the instantaneous field of view. Reflected solar radiance will also be included in at-sensor radiance if a fire is imaged during the day. Flames have lower emissivity than background materials, but the impact of flame emissivity will depend on path length through flame and the soot content of the flame (Giglio and Kendall, 2001; Riggan et al., 2004).

Dennison and Matheson (2011) tested the blackbody assumption by comparing emitted radiance acquired simultaneously by AVIRIS and the MODIS/ASTER airborne simulator (MASTER, Hook et al., 2001) over a single fire. Fire temperatures modeled using AVIRIS SWIR data were compared to fire temperatures modeled using MASTER multi-spectral MIR and TIR data. Both models assumed blackbody emission, and temperatures retrieved from the two datasets were found to be poorly correlated below 800 K. Matheson and Dennison (2012) investigated spatial scaling of AVIRIS data over four fires, and found decreases in modeled fire temperatures as spectra were aggregated up to coarser spatial resolutions. Based on fire complexity across spatial scales, uncertain emissivity, and results from previous experiments, the blackbody assumption should be regarded with caution (especially for cooler fires).

Regardless of whether blackbody emission approximates actual fire emitted radiance, maximum spectral radiance values produced by fire are an important concern for remote measurement. Sensors designed for measuring land and water surfaces typically do not have a high enough saturation threshold to adequately capture peak emission from wildfires, especially at finer spatial resolution where fire can comprise a higher percentage of individual pixels (Realmuto et al., 2015). For

example, SWIR bands in AVIRIS data have frequently saturated over the hottest parts of wildfires, especially when the spatial resolution is high (Dennison et al., 2006; Matheson and Dennison, 2012).

Detection of fire within hyperspectral data presents two challenges. Typically, hyperspectral data are acquired during the day, in which case emitted radiance must be reliably separated from the reflected solar radiance background to accurately detect fire. Also, fire may comprise a small percentage of a larger pixel, which effectively dilutes the strength of the emitted radiance signal and makes emitted radiance more difficult to separate from the reflected solar radiance background. Dennison and Roberts (2009) compared all possible normalized difference index combinations of AVIRIS bands in radiance data acquired over the 2003 Simi fire in California, USA. The presence of fire in a pixel increases spectral radiance in longer wavelength SWIR bands more rapidly than in shorter wavelength SWIR bands, and indices combining two bands spanning the range of the SWIR spectral region produced the most accurate detection of pixels containing fire. They suggested the most accurate index as the Hyperspectral Fire Detection Index (HFDI):

$$HFDI = \frac{L_{2.43 \mu\text{m}} - L_{2.06 \mu\text{m}}}{L_{2.43 \mu\text{m}} + L_{2.06 \mu\text{m}}} \quad (1)$$

where $L_{2.43 \mu\text{m}}$ (in $\text{W m}^{-2} \text{sr}^{-1} \mu\text{m}^{-1}$) is the spectral radiance around 2.43 μm , and $L_{2.06 \mu\text{m}}$ is the spectral radiance around 2.06 μm .

Dennison and Roberts (2009) further performed a sensitivity analysis on the HFDI, noting the impacts of fire temperature, subpixel fractional area, atmospheric path length and water vapor, and solar zenith angle on the index. HFDI takes advantage of an atmospheric carbon dioxide absorption feature at 2.06 μm . Reflected solar radiance experiences atmospheric carbon dioxide absorption on both the downwelling and upwelling path, while emitted radiance only experiences absorption on the upwelling path (Dennison, 2006). This difference allows improved separation of fire from the background surface, but it also effectively prohibits remote measurement of carbon dioxide emissions directly over a fire.

Excited potassium has line emission features at 0.767 and 0.770 μm . Potassium emission has been detected over fires using imaging spectrometer data, including AVIRIS (Vodacek et al., 2002) and EO-1 Hyperion (Amici et al., 2011). Finer spectral resolution improves discrimination of the potassium emission feature, but the primary limitation of this technique remains scattering and absorption by smoke within the NIR spectral region (Dennison and Roberts, 2009).

Hyperspectral temperature retrieval methods are based on a spectral mixing model approach (Giglio et al., 2003). The general form of spectral mixing models used for spectral radiance (L_λ in $\text{W m}^{-2} \text{sr}^{-1} \mu\text{m}^{-1}$) is:

$$L_\lambda = \sum_{i=1}^n f_i L_{i,\lambda} + \varepsilon_\lambda \quad (2)$$

where $L_{i,\lambda}$ is the radiance of endmember i at wavelength λ , f_i is the fraction of endmember i , n is the number of endmembers, and ε_λ is the residual error. A background endmember can include emitted radiance and/or reflected solar radiance, depending on the wavelength regions included in the model (Dennison and Matheson, 2011). Most models use a single blackbody emitted radiance endmember for fire in the model (i.e. $n = 2$). In simple two-band models, the temperature of the fire is solved for using the brightness temperature of the measured pixel and the brightness temperature of the background. In models with more than two bands, endmembers spanning a range of temperatures can be compared and subsequently the endmember that produces the lowest model error is used to assign the fire temperature to a pixel (Dennison et al., 2006). In either case, each endmember is multiplied by a fractional cover. All fractions in the model sum to one, and fractional cover of the fire endmember represents the sub-pixel fire percentage. This type of mixing model assumes that radiance from fire and background endmembers mix linearly; an assumption that is difficult to test in

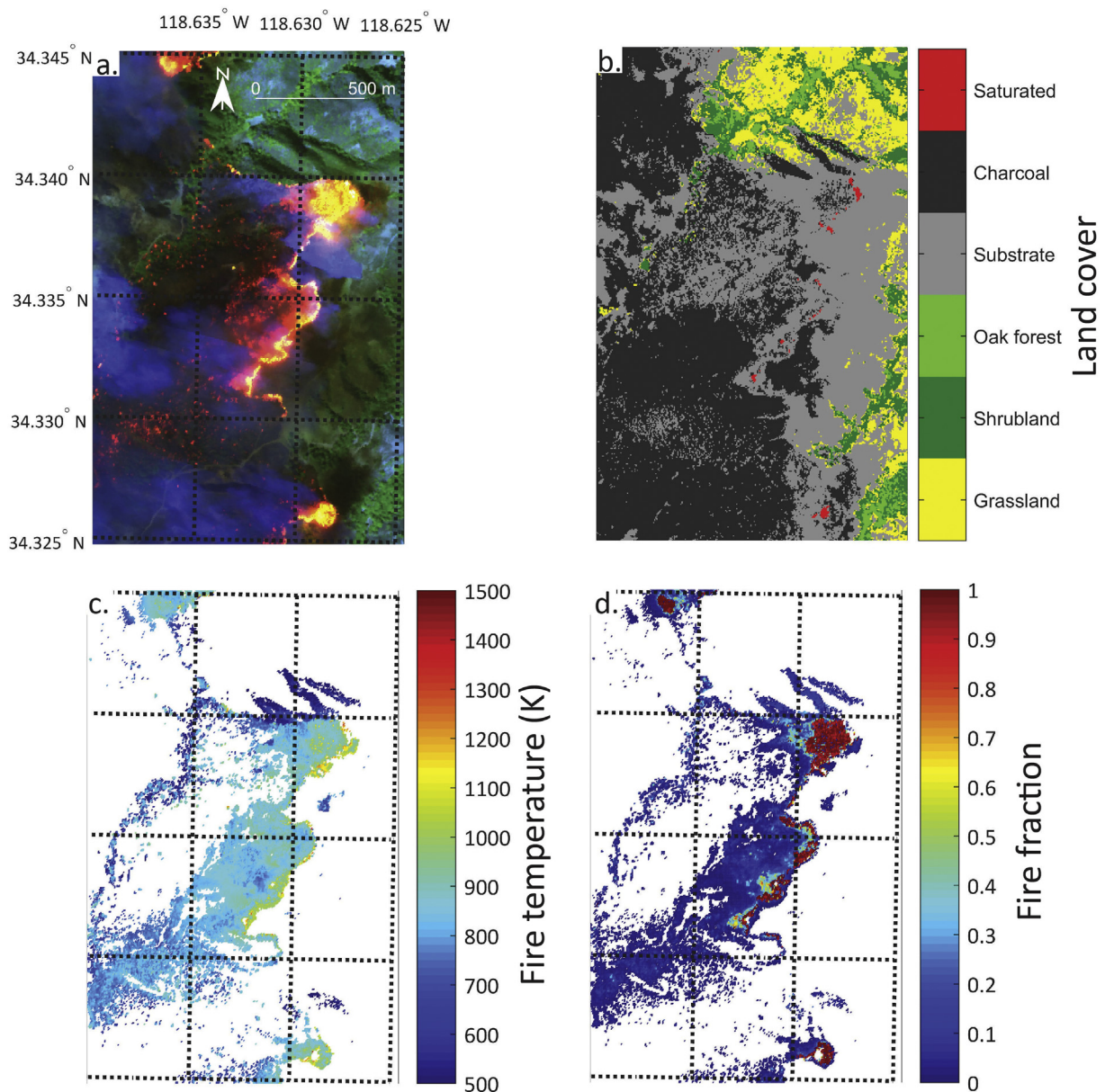


Fig. 6. a) Color composite from the Airborne Visible/Infrared Imaging Spectrometer over parts of the active 2003 Simi fire in California, USA. The composite used the bands centered at $1.70\ \mu\text{m}$ (red), $1.10\ \mu\text{m}$ (green) and $0.66\ \mu\text{m}$ (blue). b) Land cover, c) fire temperature and d) fire fraction derived from multiple endmember spectral mixture analysis after Matheson and Dennison (2012). (For interpretation of the references to color in this figure legend, the reader is referred to the web version of this article.)

reality. Mixing model retrievals of fire temperature have also frequently been applied to multispectral airborne and satellite remotely sensed data (Eckmann et al., 2008, 2009; Giglio and Schroeder, 2014; Matson and Holben, 1987; Oertel et al., 2004; Riggan et al., 2004; Zhukov et al., 2006).

The larger spectral dimensionality provided by hyperspectral data permits the application of more complex mixing models. For example, Dennison et al. (2006) created a three-endmember multiple endmember mixing model that included background endmembers for different vegetation types, soil and ash, a range of emitted radiance endmembers that included modeled atmospheric absorption, and a shade endmember that controlled for the absolute level of radiance. A major advantage of this approach is that it simultaneously produces maps of fire temperature, fire fractional area, and background land cover type (Fig. 6). Dennison and Matheson (2011) applied a similar three-endmember model, but extended both the background and fire endmembers through the MIR and TIR, and expanded the number of

potential endmembers to include both smoke and non-smoke covered backgrounds. However, the lack of reference data for validation of retrieved fire temperature remains a limitation. To date, in situ temperature measurements and hyperspectral imagery have not been collected concurrently over a fire.

2.3. Post-fire applications

2.3.1. Fire and burn severity

Fire and burn severity are defined as the degree of environmental change caused by a fire (Key and Benson, 2006). Fire severity refers to the fire-induced change without vegetation recovery effects, while burn severity represent the combined effect of the immediate fire impact and longer term recovery (Lentile et al., 2006; Morgan et al., 2014; Veraverbeke et al., 2010). Severity often refers to different ecosystem characteristics depending on ecoregion and application. In grasslands for example, combustion completeness, the ratio between combusted

and available biomass, is an important indicator of severity. In temperate ecosystems severity often refers to tree mortality, while in boreal ecosystems the depth of burning in organic soils is the main indicator of severity (Rogers et al., 2014; Turetsky et al., 2011; Veraverbeke et al., 2015). Severity data are used in two main applications. First, in the USA severity maps are operationally used by Burned Area Emergency Response (BAER) teams to diagnose risk to infrastructure and safety, and prioritize post-fire rehabilitation efforts (Eidenshink et al., 2007; Robichaud and Ashmun, 2013). Second, several studies recognize the potential of severity maps to optimize fire emissions estimates (De Santis et al., 2010; French et al., 2008). Veraverbeke and Hook (2013), Rogers et al. (2014), Veraverbeke et al. (2015, 2017) and Walker et al. (2018) implemented a remotely sensed fire severity proxy in fire-wide to regional fire emissions models. In multispectral remote sensing, the Normalized Burn Ratio (NBR, López García and Caselles, 1991) has become the most widely used spectral index for assessing fire and burn severity, often applied on Landsat imagery (French et al., 2008). NBR relates to vegetation vigor and moisture by combining NIR and SWIR reflectance. After fire, there is generally a decrease in NIR reflectance and an increase in SWIR reflectance. The differenced NBR (dNBR, Key and Benson, 2006) is obtained after bi-temporal differencing pre- and post-fire NBR images. The principles of the dNBR index are transferable to hyperspectral remote sensing. The limited availability of spaceborne hyperspectral data and the need for advance planning in airborne campaigns have resulted in very few opportunities to test the performance of a hyperspectral dNBR (Stavros et al., 2016). A rare example of such a pre-/post-fire airborne image acquisition is from van Wagtenonk et al. (2004) for a fire in Yosemite National Park, USA. They, however, found no increased sensitivity of a hyperspectral dNBR to ground measurements of severity in comparison with the Landsat-derived dNBR. Further opportunities to optimize the hyperspectral dNBR recently arose from acquisitions over two large California wildfires in areas that were part of the HypSIRI preparatory airborne campaign (Fig. 7). Schepers et al. (2014) tested several hyperspectral indices derived from a post-fire image over a heathland ecosystem in Belgium. They found that the strength and form of the relationships

between spectral indices and ground measures of severity varied by vegetation type, necessitating a vegetation stratification to derive optimal results. Jia et al. (2006b) classified three fire severity levels by applying spectral angle mapper techniques to hyperspectral data acquired over a fire in Colorado, USA.

While spectral indices can be powerful proxies of biophysical properties, they only use spectral information from two or three bands. By doing so, they do not take advantage of the wealth of spectral information available in hyperspectral remote sensing. SMA is powerful analysis tool for severity assessments with the additional advantage that the output of SMA are quantitative abundance estimates of the ground cover classes, without the need of a calibration with field data as with spectral indices (Solans Vila and Barbosa, 2010; Somers et al., 2010) (Fig. 8). SMA has been applied on multispectral post-fire imagery (Fernandez-Manso et al., 2009; Meng et al., 2017; Quintano et al., 2013; Smith et al., 2007; Veraverbeke and Hook, 2013), however, a few studies have leveraged the higher spectral resolution from hyperspectral remote sensing (Kokaly et al., 2007; Lewis et al., 2017; Lewis et al., 2011; Lewis et al., 2008; Lewis et al., 2007; Robichaud et al., 2007; Somers et al., 2016; Tane et al., 2018; Veraverbeke et al., 2014). Kokaly et al. (2007) used AVIRIS data in a hyperspectral classification of ground cover classes. Lewis et al. (2007, 2008, 2011, 2017), Robichaud et al. (2007), Veraverbeke et al. (2014), Somers et al. (2016) and Tane et al. (2018) derived cover fractions of ground classes including charcoal, ash, green vegetation, scorched vegetation, non-photosynthetic vegetation, soil and substrates. These estimates, and especially the green vegetation and charcoal fractions, were significantly correlated with ground measurements of severity in a variety of case studies in temperate and boreal ecosystems (Fig. 8b). Lewis et al. (2008) also found a relationship between ash cover derived from hyperspectral SMA and soil water repellency. Veraverbeke et al. (2014) demonstrated improvements of seven to 44% in estimating ground cover fractions from hyperspectral data compared to multispectral data. These improvements were the result of the high dimensionality of hyperspectral data that benefits discrimination between ground cover classes (Fig. 9). Tane et al. (2018) investigated the trade-off between accuracy and

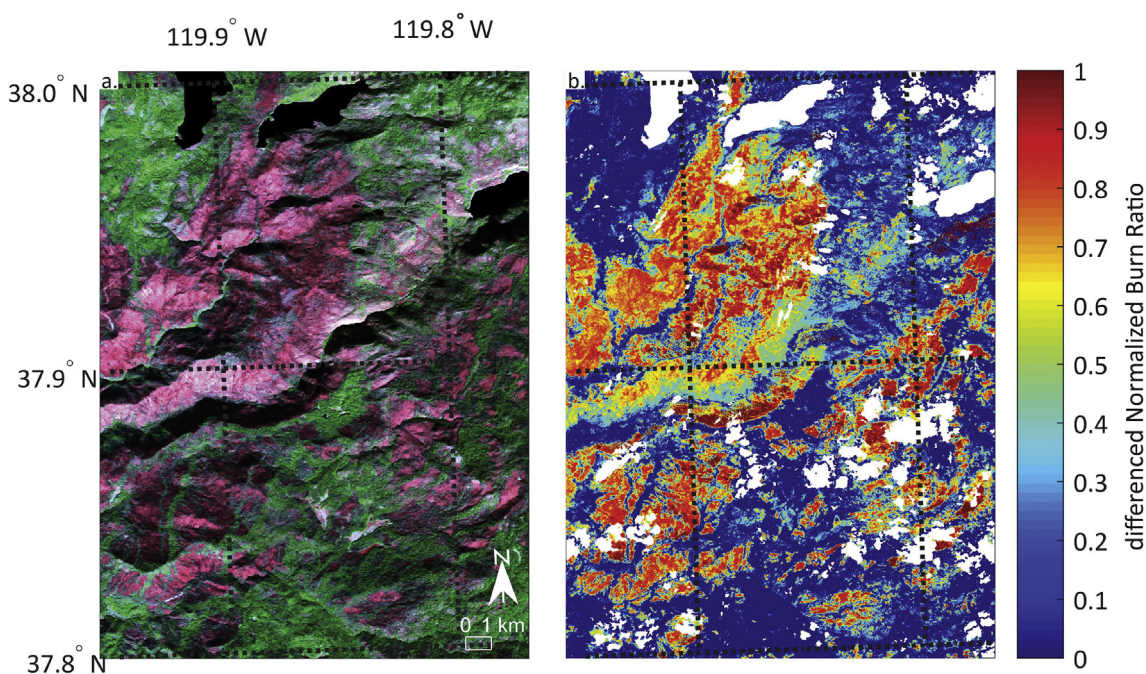


Fig. 7. a) Post-fire color composite from the Airborne Visible/Infrared Imaging Spectrometer over parts of the 2013 Rim fire in California, USA. The composite used the bands centered at 2.10 μm (red), 0.88 μm (green) and 0.69 μm (blue). b) Hyperspectral differenced Normalized Burn Ratio over the same area. Clouds and water bodies were masked and are depicted in white. (For interpretation of the references to color in this figure legend, the reader is referred to the web version of this article.)

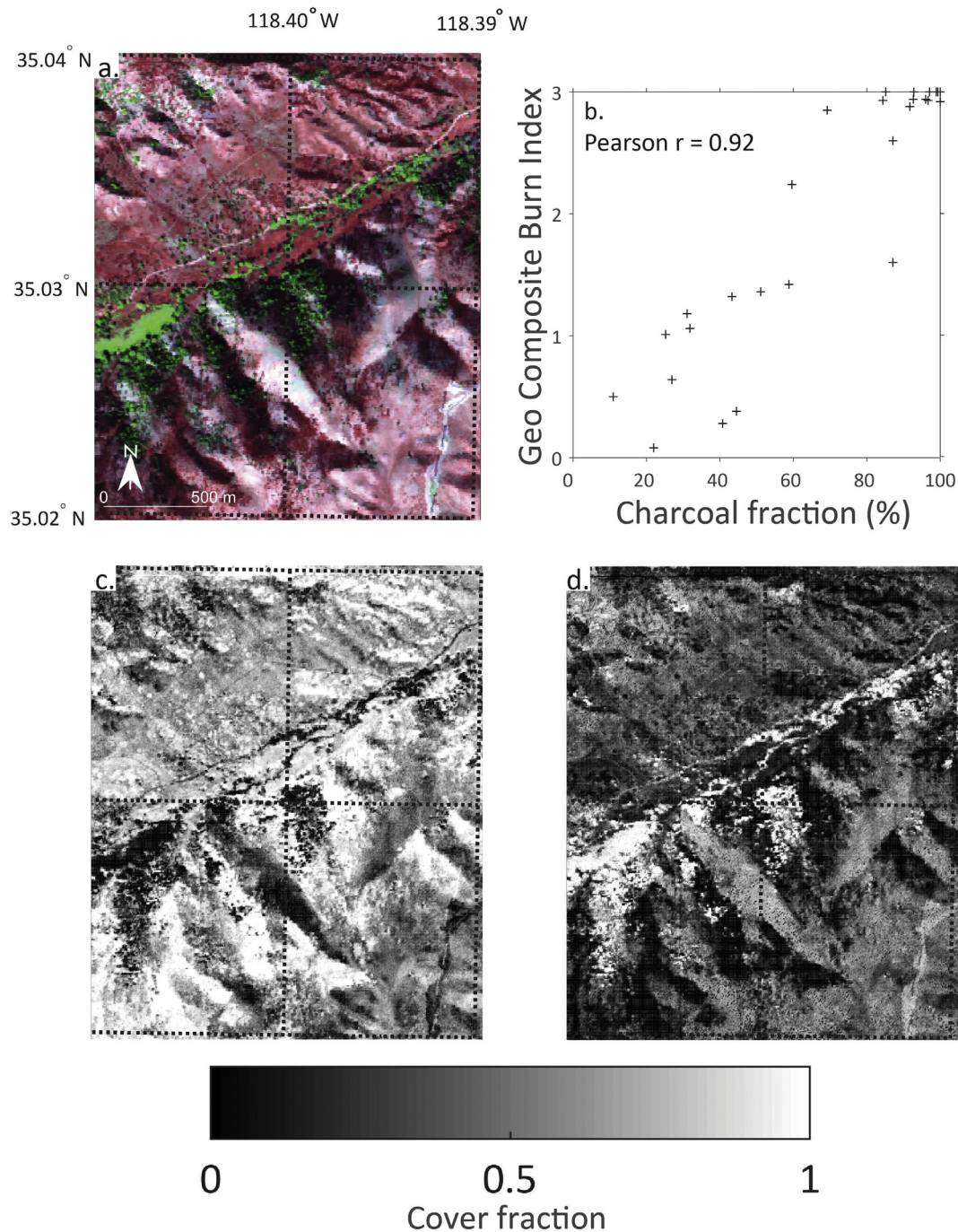


Fig. 8. a) Post-fire color composite from the Airborne Visible/Infrared Imaging Spectrometer over parts of the 2011 Canyon fire in California, USA. The composite used the bands centered at 2.10 μm (red), 0.88 μm (green) and 0.69 μm (blue). b) Correlation between charcoal fraction and the Geo Composite Burn Index, a field measurements of fire severity (De Santis and Chuvieco, 2009). c) Fractional cover maps of charcoal and (d) green vegetation derived from spectral mixture analysis (after Veraverbeke et al., 2014). (For interpretation of the references to color in this figure legend, the reader is referred to the web version of this article.)

computational efficiency by applying different band and endmember selection techniques. Discrimination of charcoal hinges on its characteristic low reflectance for NIR wavelengths (Fig. 9a). Green vegetation is spectrally different than other ground cover classes due its combined high NIR and low SWIR reflectance (Fig. 9b). Separability of NPV from substrate is usually more challenging in visible to SWIR spectral regions (Fig. 9cd) (Roberts et al., 1993). As an alternative to empirical and often site-specific spectral indices and SMA, Chuvieco et al. (2006), De Santis et al. (2009) and De Santis and Chuvieco (2007) developed a physically based RTM to map burn severity. The model accounted for fire-induced changes in soil color, vegetation color (green

and brown), and vegetation cover. Although the model is applicable to hyperspectral imagery (Chuvieco et al., 2006), it has so far only been applied in multispectral case studies.

2.3.2. Vegetation recovery

Various fire-affected variables can be measured and modeled in post-fire environments. Following the prior definition of burn severity, vegetation recovery can be part of a severity assessment (Lentile et al., 2006; Morgan et al., 2014; Veraverbeke et al., 2010). Post-fire species structure and composition, and vegetation succession are crucial variables in understanding ecosystem responses to fire disturbance and

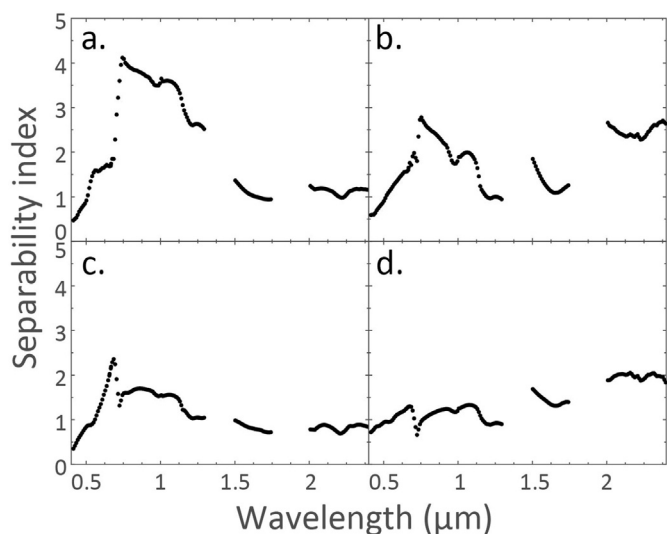


Fig. 9. Spectral separability of a) charcoal, b) green vegetation, c) non-photosynthetic vegetation and d) substrate. Spectral separability was calculated from the between- and within-class variability of endmember spectra (Somers et al., 2009; Veraverbeke et al., 2014). (For interpretation of the references to color in this figure legend, the reader is referred to the web version of this article.)

climate change (Capitaino and Carcaillet, 2008; Chu and Guo, 2013). Especially in forest ecosystems, the spatial distribution of various forest components, such as tree height and sapling density, defines forest structure while species richness and abundance characterize forest composition and biodiversity (McElhinny et al., 2005).

The terms vegetation recovery, vegetation regrowth, vegetation regeneration are used, often interchangeably, to describe the various stages of post-fire vegetation succession in fire-affected ecosystems (Johnstone and Kasischke, 2005; Mitri and Gitas, 2013; Veraverbeke et al., 2012b). These terms refer to the recovery process of species or ecosystems to a pre-disturbance condition. Fires can also lead to permanent changes in vegetation composition and structure, decreased vegetation cover, biomass loss and the alteration of landscape patterns (Pérez-Cabello et al., 2009). Consequently, detailed monitoring of post-

fire vegetation dynamics helps define the ecological impact of fires on ecosystem functioning, and allows implementation of effective restoration measures (Gitas et al., 2012; Gouveia et al., 2010; van Leeuwen et al., 2010; Veraverbeke et al., 2012b). Fire severity, post-fire meteorological conditions, fuel type, topography and soil properties are all factors that influence recovery patterns (Moreira et al., 2009; Pausas and Fernández-Muñoz, 2012; Veraverbeke et al., 2010).

Broadband multispectral remote sensing has been used extensively to assess post-fire vegetation recovery at various temporal and spatial scales (Díaz-Delgado et al., 2003; Goetz et al., 2006; Gouveia et al., 2010; Leon et al., 2012). The existence of long time series of multispectral imagery spanning consecutive decades, combined with free data distribution policies have substantially increased its use in post-fire recovery applications. Most of these studies rely on vegetation abundance proxies derived from vegetation indices like the Normalized Difference Vegetation Index (NDVI) and NBR, often processed using advanced trajectory analysis algorithms (Katagis et al., 2014; Leon et al., 2012; Storey et al., 2016; Zhao et al., 2016).

In a preliminary study on monitoring post-fire succession in California's Santa Monica mountains, AVIRIS-derived vegetation indices were tested for their capability to detect variations in the photosynthetic activity of chaparral (Qiu et al., 1998). The NDVI was used along with specific narrowband indices, the Photochemical Reflectance Index (PRI, Gamon et al., 1997) (PRI) and the Water Band Index (WBI). Findings indicated that including narrowband indices eased detection of sensitive changes in photosynthetic activity that were not associated with changes in canopy structure. Multitemporal AVIRIS imagery was used in another post-fire vegetation regeneration in the Santa Monica mountains (Riaño et al., 2002). Riaño et al. (2002) found that GV fraction performed equally well in both northern mixed chaparral and south coastal sage scrub communities, as opposed to NDVI measurements that were influenced by phenological variations. Also in California, Somers et al. (2016) demonstrated the utility of MESMA-derived cover fraction to monitor post-fire vegetation recovery (Fig. 10). In a similar application, multitemporal airborne hyperspectral (AHS) imagery and SMA were combined to monitor post-fire recovery in Spain (Huesca et al., 2013).

To track ecological changes caused by fire across multiple spatial and temporal scales, Lewis et al. (2017) made combined use of airborne

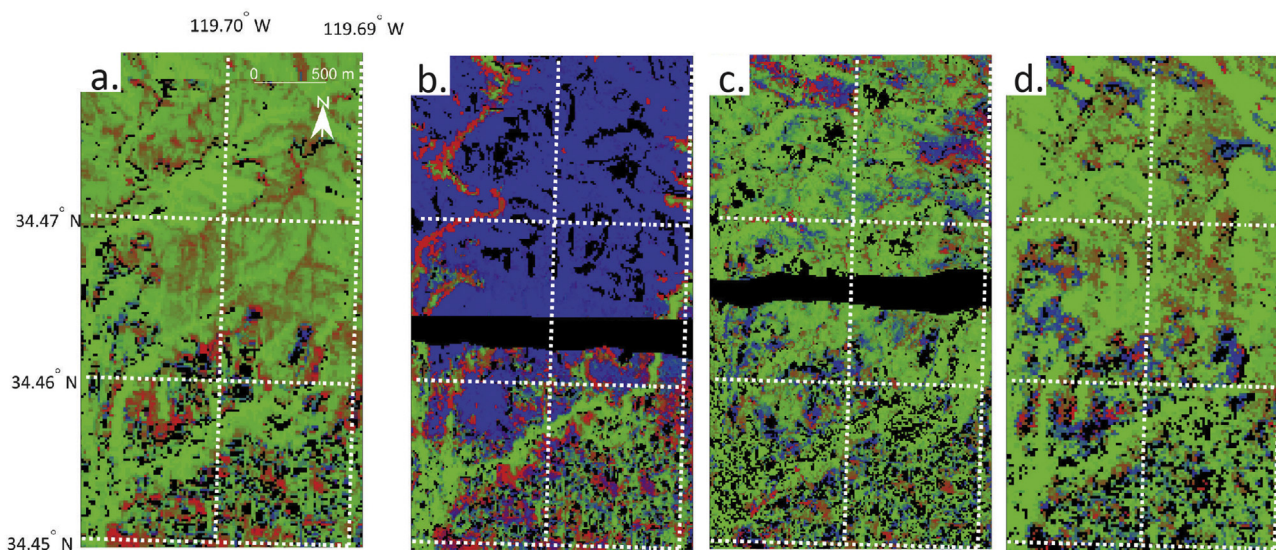


Fig. 10. Time series of surface composition between 2004 and 2013 in the area of the 2009 Jesusita fire in California, USA, as derived from Airborne Visible/Infrared Imaging Spectrometer a) on August 6, 2004, b) just after the fire on August 26, 2009, c) on April 30, 2010, and d) on June 6, 2013. The false color composites input non-photosynthetic vegetation (red), green vegetation (green) and substrate and ash (blue) cover fractions retrieved from multiple endmember spectral mixture analysis. Suboptimal retrievals and missing data were masked in black (after Somers et al., 2016). (For interpretation of the references to color in this figure legend, the reader is referred to the web version of this article.)

hyperspectral data, spaceborne high, i.e. QuickBird, and medium, i.e. Landsat, spatial resolution multispectral imagery collected on anniversary dates spanning ten years after three large wildfires in Montana, USA, 2003. They used MESMA to derive post-fire char, soil, GV, and NPV fraction maps at different recovery times. Retrievals from hyperspectral imagery had stronger correlations with ground measurements one year post-fire, and with vegetation canopy data ten year post-fire. Mitri and Gitas (2010, 2013) applied object-based image analysis on single date EO-1 Hyperion images for classifying forest regeneration and vegetation recovery in fire-affected areas on the Greek island of Thasos. Vegetation indices derived from Hyperion were also useful for estimating post-fire recovery in Mato Grosso in the southern Amazon in Brazil (Numata et al., 2011). In this study, selected narrowband indices outperformed the NDVI in detecting subtle changes in the physiological properties of disturbed forests.

Despite the limited number of applications due to data limitations, hyperspectral data provide opportunities for post-fire monitoring that are not supported by broadband multispectral imagery. The reviewed applications mostly hinged on single date or a small number of hyperspectral airborne or spaceborne images. Current limitations in deploying airborne campaigns limit further exploration of the possibilities that arise from hyperspectral data in post-fire recovery studies. The upcoming hyperspectral satellite missions in an era of open data policies will enable more systematic exploitation of hyperspectral information in post-fire monitoring studies.

3. Future perspectives

3.1. Automated image-based endmember extraction for spectral mixture analysis

SMA, and in particular MESMA that accounts for within-class endmember variability, is a popular image analysis technique in all phases of the fire disturbance continuum: before, during and after the fire. In the studies reviewed here, endmember spectra were most often measured in the field using a field spectroradiometer, or derived from the imagery or existing spectral libraries (Baldrige et al., 2009). This approach was feasible and effective for local-scale studies as the ones based on the limited air- and spaceborne hyperspectral data opportunities reviewed here. The large datasets that will originate from the upcoming spaceborne hyperspectral missions, however, require automated and image-specific endmember bundle retrievals. The importance of this concept has been previously discussed, and image-based endmember retrieval techniques have been developed (Bateson et al., 2000; Roth et al., 2012; Somers et al., 2012), yet without large scale application and thorough validation over space and time. Techniques like MESMA may be applied to generate standardized products for future hyperspectral missions to for example quantify GV, NPV and substrate fractions. However, to achieve this, spectral libraries and revised methods are required to provide fractions that are comparable across large geographic regions, multiple years and across seasons (Dudley et al., 2015). Fire studies focused on pre-fire fuel type and condition or post-fire recovery will likely be able to leverage information from these products. Specific attention will be required for active fire and post-fire severity studies because these applications need additional endmembers that are foreign to vegetation or substrate studies. Spectral signatures of active fires can be modeled from the Planck function for different temperatures (Fig. 5). Inclusion of the active fire endmember could consist of spectral signatures from multiple temperatures, or could capitalize upon iterative optimization techniques. Fire severity studies need the inclusion of a charcoal or ash endmember (e.g. Lewis et al., 2017), which could simply be implemented by extending the three-endmember model of GV, NPV and substrate to a four-endmember model that adds the charcoal/ash endmember. The implementation of this addition could be restricted to burned area only, especially when a separate burned area retrieval would be available

from the suite of satellite products (Tane et al., 2018).

3.2. Radiative transfer models

RTMs have the potential to provide physically-based retrieval of plant biophysical and biochemical properties, including fuel moisture (Casas et al., 2014; Jurdao et al., 2013; Riano et al., 2005; Yebra et al., 2018) and fire severity (Chuvieco et al., 2006; De Santis et al., 2009; De Santis and Chuvieco, 2007). Modeling studies have demonstrated that fuel moisture content can be retrieved from remotely sensed data using RTM inversion (Bowyer and Danson, 2004; Ceccato et al., 2001; Riano et al., 2005). Application of RTMs to hyperspectral data have not yet demonstrated conclusive gains in accuracy over empirical methods for estimating fuel moisture (Casas et al., 2014), while RTMs have not yet been applied to hyperspectral imagery for fire severity assessments. Empirical estimation techniques have the advantage of allowing for site-dependent variation in the relationship between reflectance and fuel moisture content, while RTMs may be more promising for developing continental to global-scale fuel moisture retrievals (Yebra et al., 2018). Upcoming spaceborne hyperspectral missions will deliver much higher temporal frequency than airborne sensors have previously provided, which should improve both RTM and empirical fuel moisture retrievals. RTM methods can use time series data to estimate dry matter content during the dry season (Riano et al., 2005), and denser time series data may also reduce uncertainty in empirical relationships. Operational fuel moisture monitoring may require higher temporal resolution than provided by upcoming spaceborne hyperspectral sensors. The possibility of having multiple coincident hyperspectral sensors in different orbits, however, may increase the temporal resolution of hyperspectral imagery. In case the temporal sampling remains insufficient for operational mapping of fuel moisture, spaceborne hyperspectral fuel moisture retrievals may be useful for calibration and validation of retrievals based on imagery with lower spatial and/or spectral resolution (Roberts et al., 2003; Trombetti et al., 2008). For fire severity mapping, the temporal constraint is less stringent since only one post-fire image is needed.

3.3. Optimizing hyperspectral fire severity indices

Hyperspectral data are powerful for fire severity assessments because they allow accurate within-pixel fractional cover estimates of ground cover classes, among other charcoal, that are indicative for severity (Lewis et al., 2017; Meng et al., 2017; Veraverbeke et al., 2014). A more traditional method for mapping fire and burn severity is the dNBR. The dNBR has the advantage of conceptual simplicity and computational efficiency, and may therefore complement more sophisticated retrievals (Veraverbeke and Hook, 2013). The Landsat dNBR is the most often used approach to assess fire and burn severity (French et al., 2008; Key and Benson, 2006). In multispectral remote sensing, commonly one band combination per sensor allows the calculation of the dNBR. In hyperspectral remote sensing, however, several band combinations lead to multiple dNBR definitions that are slightly different. It may be possible that there exists an optimal combination of NIR and SWIR narrowbands. So far, this exercise has not been undertaken partly because of the limited availability of pre- /post-fire image pairs required for dNBR calculation (Stavros et al., 2016). However, opportunities that arise from two recent California wildfires that were imaged by AVIRIS as part of the HypSIRI preparatory airborne campaign allow such an investigation. Investigations could focus on relationships with field measurements of severity and spectral index optimality for multiple band combinations (Pinty and Verstraete, 1992; Roy et al., 2006; Thenkabail et al., 2002).

3.4. Synergy between hyperspectral and light detection and ranging (LiDAR) data

Hyperspectral and LiDAR data are complementary. Hyperspectral data can discriminate between fuel type and condition, yet LiDAR data can provide additional information regarding the three-dimensional (3D) structure of fuels (Riaño et al., 2003) and ground surface. By doing so, the synergy between hyperspectral and LiDAR technologies can effectively be named 3D imaging spectroscopy. This synergy has been explored in a few pre-fire applications (Colgan et al., 2012; Levick et al., 2015; Stavros et al., 2018; Varga and Asner, 2008). Colgan et al. (2012) used LiDAR to identify individual tree crowns and estimate canopy height, while hyperspectral data guided tree species discrimination. This approach was successful for mapping fuels in Kruger National Park in South Africa. Levick et al. (2015) applied similar methods in the same study area and found that areas with higher fire frequency were associated with reduced tree cover and shifts in canopy height distribution. Varga and Asner (2008) combined hyperspectral and LiDAR data to map the 3D structure of grass fuels in Hawaii Volcanoes National Park, USA. They therefore combined fractional cover estimates of NPV from SMA on hyperspectral data with canopy heights from LiDAR. Their derived fire fuel index is a proxy of flammability and fire spread potential. Stavros et al. (2018) combined hyperspectral and structural data to map fuels in a Californian landscape.

Combined hyperspectral and LiDAR data have rarely been exploited in post-fire applications. This research gap is likely explained by shortages in synergistic image acquisitions, especially from both before and after the fire. Post-fire charcoal fractional cover or dNBR derived from hyperspectral images combined with changes in canopy height distribution could significantly refine carbon emission estimates from fires especially if these post-fire retrievals are supplemented with knowledge on pre-fire fuel composition and amount. Chen (2017) provided some first insight on complementarities between the dNBR and MESMA fractional covers derived from hyperspectral imagery, and canopy height derived from LiDAR in a post-fire environment (Fig. 11). The MESMA output allows greater separation in riparian areas compared to the dNBR, whereas the canopy heights from LiDAR are indicative of residual standing biomass, even in areas mapped as ash by MESMA. Such synergistic research opportunities are rare within airborne campaigns, however, airborne hyperspectral and LiDAR data from before and after fire cover large parts of two recent California fires and present an ideal case study (Stavros et al., 2016). Meng et al. (2018) recently combined hyperspectral and LiDAR imagery to estimate species-level post-fire recovery responses to different fire severity levels.

3.5. Hyperspectral thermal applications

Hyperspectral TIR data can provide complementary information to visible and SWIR data in fire applications. These applications include detection of water- and temperature-induced stress in plant species based on spectral changes in TIR emissivity (Buitrago et al., 2016; Meerdink et al., 2016; Ullah et al., 2012), and the detection and quantification of particulate and gaseous emissions from active fires (Hulley et al., 2016; Kuai et al., 2016). Identifying plant species (Meerdink et al., 2016; Ullah et al., 2012) and detection of water- and temperature-induced stress in plant species (Buitrago et al., 2016) using spectral emissivity have so far only been demonstrated with laboratory measurements in controlled environments, but have the potential to provide information on plant stress and moisture content, and thus pre- and post-fire fuel condition (Neinavaz et al., 2017). For example, Buitrago et al. (2016) found that plants exposed to water and temperature stress showed significant changes in their TIR spectra, which were linked to changes in the cuticle thickness and structure. More work is required to apply these methods to hyperspectral TIR data from air- or spaceborne platforms.

Hyperspectral TIR measurements over active fires are presently

limited due to detector saturation limits and the lack of suitable air- and spaceborne instrumentation. Wildfires have not been a prime target for most airborne thermal missions in the past, and wildfire occurrence is ephemeral limiting acquisition windows for airborne campaigns. The Hyperspectral Thermal Emission Spectrometer (HyTES), an airborne imaging spectrometer with high spectral resolution (256 bands between 7.5 and 12 μm), wide swath (1–2 km), and high spatial resolution (2 m at 1 km altitude flying height), has acquired data over four small active fires in California, USA since deployment in 2013, but these have only been considered targets of opportunity acquired en route to other destinations. Hyperspectral satellite sensors like the Infrared Atmospheric Sounding Interferometer (IASI, Aires et al., 2002), the Tropospheric Emission Spectrometer (TES, Beer, 2006), and the Atmospheric Infrared Sounder (AIRS, Tobin et al., 2006) have the capability to observe large gaseous emissions from fires, however, they are limited by their coarse spatial resolutions of 10 km or more, and insensitivity to near-surface concentrations due to sensor saturation issues. Airborne hyperspectral TIR sensors such as HyTES on the other hand have the imaging capability to detect gaseous emission sources at pixel sizes of a few meters, and have sufficient spectral information to resolve the spectral absorption signatures of a variety of different trace gases including methane (CH_4), ammonia (NH_3), hydrogen sulfide (H_2S), sulfur dioxide (SO_2), nitrogen dioxide (NO_2) and nitrous oxide (N_2O) (Hulley et al., 2016; Kuai et al., 2016). The primary gas species emitted from wildfires, CO_2 and CO , do not exhibit spectral absorption features in the TIR region, however, other biomass burning gases such as CH_4 and NH_3 are detectable with high confidence (Hulley et al., 2016). Biomass burning is a major source of atmospheric NH_3 (Hegg et al., 1988; Whitburn et al., 2015). Examples of the absorption features of CH_4 and NH_3 are shown in Fig. 12. Airborne hyperspectral TIR data have the ability to discriminate these gases within a single plume pixel. A further unique advantage of TIR data for fire applications is that night-time observations allow easier detection of gas emissions since the collapsed nocturnal planetary boundary layer results in higher near-surface concentrations. In addition, the ability to detect fires is greater at night since during the day active fires can be confused with warm ground surfaces, especially with lower spatial resolution sensors.

During active fires, hyperspectral TIR data have the ability to quantify surface and near-surface air temperature in the vicinity of the fire, and downwind concentrations of NH_3 and CH_4 , with an error between 50 and 80% for NH_3 and between 20 and 25% for CH_4 (Kuai et al., 2016). HyTES detected a NH_3 plume over the Gulch fire, a small fire in southern Utah, USA, in July 2014 (Fig. 13). The fire plume exhibited NH_3 mole fraction enhancements of up to 5.5 ppb. This is approximately 10 ppb lower than emissions from the El Segundo natural gas power plant in Los Angeles, USA, observed in prior HyTES campaigns. The magnitude of NH_3 and particulate emissions are primarily determined by combustion type (Liu et al., 2014; Reid et al., 2005; Yokelson et al., 1997). Incomplete combustion products include CO , CH_4 , NH_3 , C2–C3 hydrocarbons, methanol (CH_3OH), formic and acetic acids, and formaldehyde (CH_2O) (Bertschi et al., 2003; Yokelson et al., 1997). The observed NH_3 values are within expectations for the creeping and smoldering conditions and incomplete combustion of the Gulch fire.

Because TIR spectrometers rely on the thermal emission and thermal contrast between the ground and gas for detection, particulate scattering from smoke has little effect on the signal. This suggests potential for combined analysis of both the particulate and gaseous emissions from fires by flying HyTES with a multi-angle polarimeter imager such as the Airborne Multi-angle Spectro Polarimetric Imager (AirMSPI, Diner et al., 2013). AirMSPI is an airborne prototype instrument used for obtaining multi-angle polarization imagery. AirMSPI could be used to assess the relative contribution of organic, non-organic, and black carbon particles to the total airborne particle emissions (Kalashnikova et al., 2018), while HyTES could provide information on concentrations of gaseous emissions and temperature. Synergistic use of

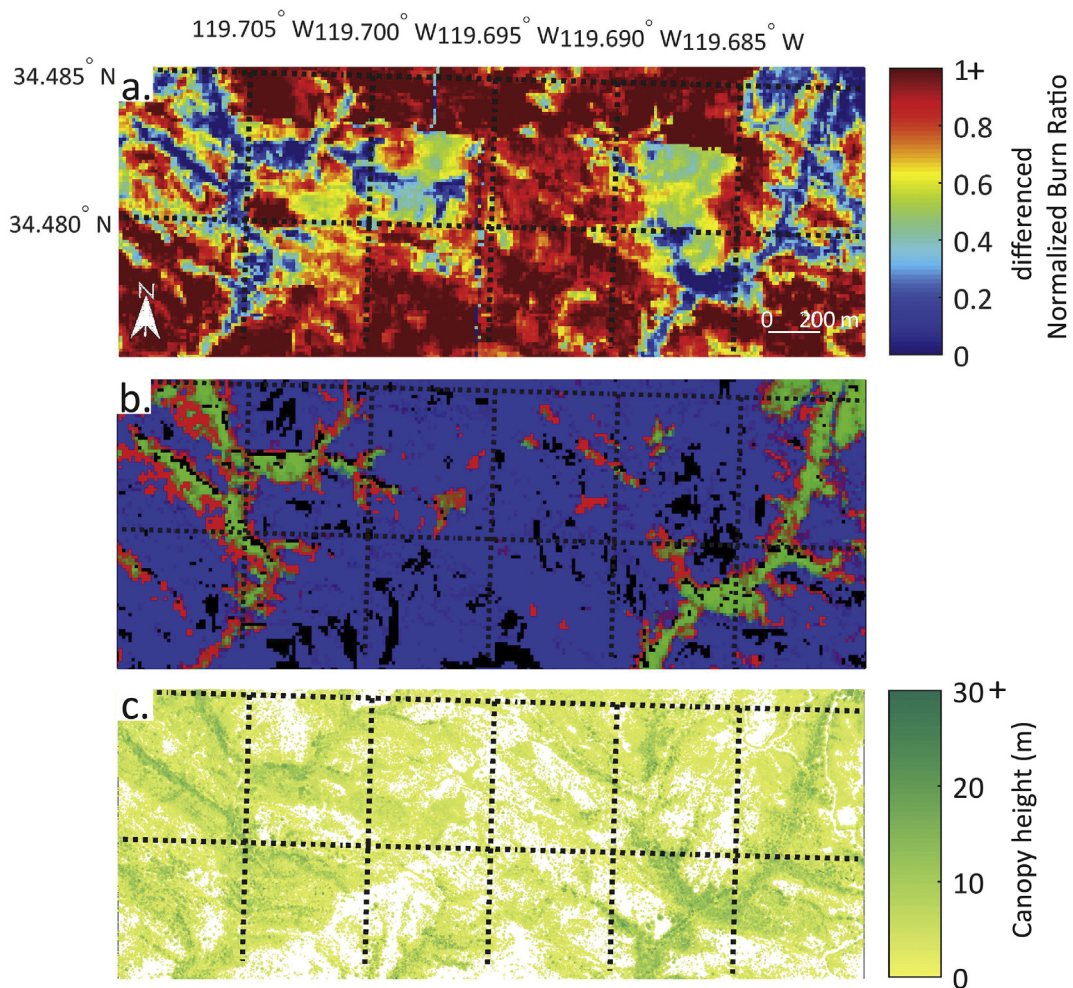


Fig. 11. a) Hyperspectral differenced Normalized Burn Ratio and b) surface composition (as in Fig. 11b) derived from in the 2009 Jesuita burned area in California, USA, as derived from Airborne Visible/Infrared Imaging Spectrometer. c) Canopy height derived from an airborne light detection and ranging acquisition in December 2009 (after Chen, 2017).

hyperspectral thermal and multi-angle observations would help constrain biomass burning emissions and particulate composition of smoke to help model and predict the impacts of future emissions on air quality and climate change. Another interesting synergy is between

hyperspectral VSWIR, MIR and TIR data. The VSWIR spectral region is more sensitive to high temperatures between approximately 800 and 1500 K, and thus ideally suited for hot flaming fires. The MIR and TIR spectral regions in contrast are more sensitive to lower temperatures

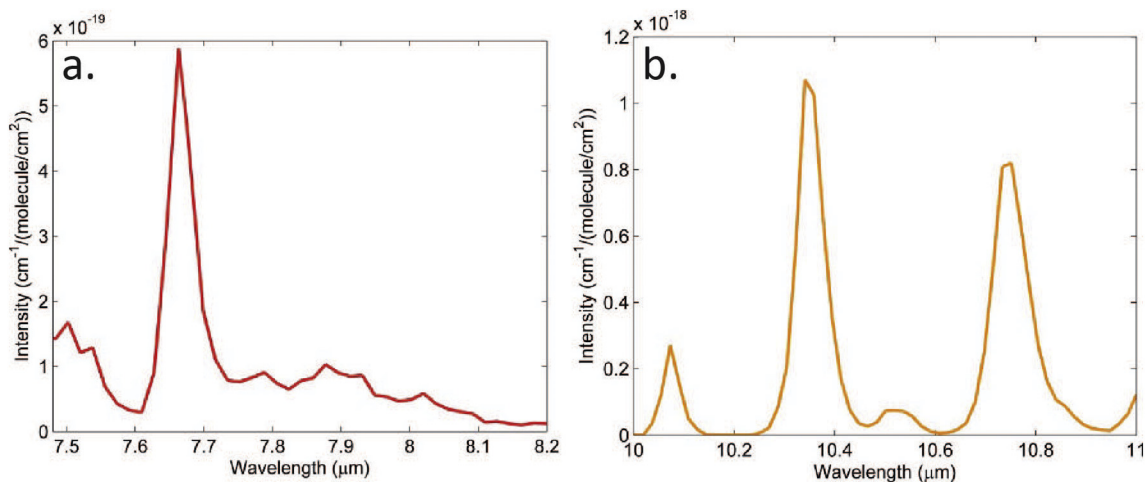


Fig. 12. Absorption features of a) CH₄ and b) NH₃ extracted from the high-resolution transmissions molecular absorption 2012 database (HITRAN, Rothman et al., 2013) convolved to spectral response functions of the Hyperspectral Thermal Emission Spectrometer. Spectral regions with high intensity represent absorption features.

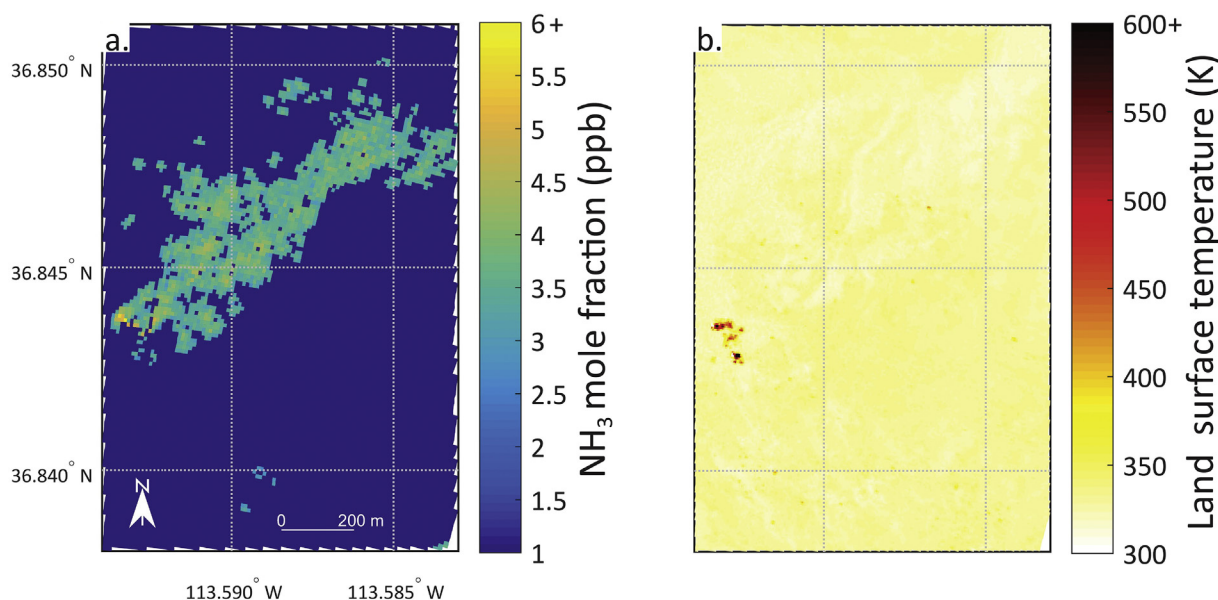


Fig. 13. a) An ammonia (NH_3) plume from fire emissions and b) land surface temperature over the active fire region in Utah, USA, in July 2014 derived from Hyperspectral Thermal Emission Spectrometer imagery.

between approximately 300 and 800 K, and thus better suited for cooler smoldering fires. The combined use of hyperspectral VSWIR, MIR and TIR data thus offers opportunities to better characterize the full range of fire temperatures on Earth.

4. Conclusions

Hyperspectral remote sensing has proven utility in all temporal stages of the fire disturbance continuum. In pre-fire applications, hyperspectral data allows detailed assessment of fuel type and condition. Fire temperatures and gaseous emissions can be determined from active fires with hyperspectral data. After the fire, hyperspectral information from charcoal, ash and vegetation are indicative for fire severity and ecosystem recovery. Improvements from hyperspectral imagery come from its ability to capture narrow spectral features, e.g. water absorption features for fuel moisture estimations, and/or better constraints on algorithms because of the higher spectral data dimensionality. So far, hyperspectral fire applications have almost exclusively leveraged airborne data in the visible to short-wave infrared. The number of studies is limited because airborne campaign planning generally does not include ephemeral fire occurrence. Despite the limited number of studies, these examples demonstrate the feasibility and maturity of hyperspectral data processing for large scale applications when such datasets would become available from spaceborne platforms. Scheduled missions like EnMAP, HyspIRI and PRISMA will provide opportunities to further explore linkages between ecosystem properties and fires at regional to global scales. The maturity of applications based on visible to short-wave infrared regions is supplemented by upcoming innovative developments in the mid to thermal infrared regions. Recent airborne hyperspectral thermal infrared developments show the potential for significant advances in retrieving fire temperature and gaseous emissions. Further research should focus on preparing readiness of processing techniques for large scale hyperspectral applications in the visible to short-wave infrared, increasing airborne acquisition and data exploration of fires with hyperspectral thermal data, and building synergistic capacities between hyperspectral data and structural data from light or radio detection and ranging instruments.

Acknowledgements

We thank three anonymous reviewers and the editor Prof. Dr.

Emilio Chuvieco for their suggestions on the initial manuscript. We thank Natalie Queally for providing input for the pre-fire figures, Erin Wetherley for the post-fire recovery figure and Mingquan Chen for the figure about the synergy between hyperspectral and light detection and ranging imagery. Dr. Ran Meng was supported by the United States Department of Energy contract No. DE-SC0012704 to Brookhaven National Laboratory. Parts of this work were carried out at the Jet Propulsion Laboratory (JPL), California Institute of Technology, under a contract with National Aeronautics and Space Administration. Copyright 2018 California Institute of Technology. All rights reserved.

References

- Adams, J.B., Smith, M.O., Johnson, P.E., 1986. Spectral mixture modeling: a new analysis of rock and soil types at the Viking Lander 1 Site. *J. Geophys. Res.* 91, 8098. <http://dx.doi.org/10.1029/JB091iB08p08098>.
- Agee, J.K., 1993. *Fire Ecology of Pacific Northwest Forests*. Island Press, Washington, D.C.
- Aires, F., Rossow, W., Scott, N., Chedin, A., 2002. Remote sensing from the infrared atmospheric sounding interferometer instrument 2. Simultaneous retrieval of temperature, water vapor, and ozone atmospheric profiles. *J. Geophys. Res.* 107, 4620. <http://dx.doi.org/10.1029/2001JD001591>.
- Al-Moustafa, T., Armitage, R.P., Danson, F.M., 2012. Mapping fuel moisture content in upland vegetation using airborne hyperspectral imagery. *Remote Sens. Environ.* 127, 74–83. <http://dx.doi.org/10.1016/j.rse.2012.08.034>.
- Amici, S., Wooster, M.J., Piscini, A., 2011. Multi-resolution spectral analysis of wildfire potassium emission signatures using laboratory, airborne and spaceborne remote sensing. *Remote Sens. Environ.* 115, 1811–1823. <http://dx.doi.org/10.1016/j.rse.2011.02.022>.
- Andela, N., van der Werf, G.R., 2014. Recent trends in African fires driven by cropland expansion and El Niño to La Niña transition. *Nat. Clim. Chang.* 4, 791–795. <http://dx.doi.org/10.1038/nclimate2313>.
- Andela, N., Morton, D.C., Giglio, L., Chen, Y., van der Werf, G.R., Kasibhatla, P.S., DeFries, R.S., Collatz, G.J., Hantson, S., Kloster, S., Bachelet, D., Forrest, M., Lasslop, G., Li, F., Manganon, S., Melton, J.R., Yue, C., Randerson, J.T., 2017. A human-driven decline in global burned area. *Science* 80, 356.
- Anderson, H.E., 1970. Forest fuel ignitability. *Fire. Technol* 6, 312–319. <http://dx.doi.org/10.1007/BF02588932>.
- Anderson, M.C., Neale, C.M.U., Li, F., Norman, J.M., Kustas, W.P., Jayanthi, H., Chavez, J., 2004. Upscaling ground observations of vegetation water content, canopy height, and leaf area index during SMEX02 using aircraft and Landsat imagery. *Remote Sens. Environ.* 92, 447–464. <http://dx.doi.org/10.1016/j.rse.2004.03.019>.
- Baldrige, A.M., Hook, S.J., Grove, C.I., Rivera, G., 2009. The ASTER spectral library version 2.0. *Remote Sens. Environ.* 113, 711–715. <http://dx.doi.org/10.1016/j.rse.2008.11.007>.
- Barbosa, P.M., Grégoire, J.-M., Pereira, J.M.C., 1999. An algorithm for extracting burned areas from time series of AVHRR GAC data applied at a continental scale. *Remote Sens. Environ.* 69, 253–263. [http://dx.doi.org/10.1016/S0034-4257\(99\)00026-7](http://dx.doi.org/10.1016/S0034-4257(99)00026-7).
- Bartholomé, E., Belward, A.S., 2005. GLC2000: a new approach to global land cover mapping from Earth observation data. *Int. J. Remote Sens.* 26, 1959–1977. <http://dx.doi.org/10.1080/01621670500000000>.

- doi.org/10.1080/01431160412331291297.
- Bateson, C.A., Asner, G.P., Wessman, C.A., 2000. Endmember bundles: a new approach to incorporating endmember variability into spectral mixture analysis. *IEEE Trans. Geosci. Remote Sens.* 38, 1083–1094. <http://dx.doi.org/10.1109/36.841987>.
- Beer, R., 2006. TES on the aura mission: scientific objectives, measurements, and analysis overview. *IEEE Trans. Geosci. Remote Sens.* 44, 1102–1105. <http://dx.doi.org/10.1109/TGRS.2005.863716>.
- Bertschi, I., Yokelson, R.J., Ward, D.E., Babbitt, R.E., Susott, R.A., Goode, J.G., Hao, W.M., 2003. Trace gas and particle emissions from fires in large diameter and belowground biomass fuels. *J. Geophys. Res. Atmos.* 108. <http://dx.doi.org/10.1029/2002JD002100>.
- Boer, M., Macfarlane, C., Norris, J., Sadler, R., Wallace, J., Grierson, P., 2008. Mapping burned areas and burn severity patterns in SW Australian eucalypt forest using remotely-sensed changes in leaf area index. *Remote Sens. Environ.* 112, 4358–4369. <http://dx.doi.org/10.1016/j.rse.2008.08.005>.
- Bond, W., Keeley, J., 2005. Fire as a global 'herbivore': the ecology and evolution of flammable ecosystems. *Trends Ecol. Evol.* 20, 387–394. <http://dx.doi.org/10.1016/j.tree.2005.04.025>.
- Bowman, D.M.J.S., Balch, J.K., Artaxo, P., Bond, W.J., Carlson, J.M., Cochrane, M.A., D'Antonio, C.M., Defries, R.S., Doyle, J.C., Harrison, S.P., Johnston, F.H., Keeley, J.E., Krawchuk, M.A., Kull, C.A., Marston, J.B., Moritz, M.A., Prentice, I.C., Roos, C.I., Scott, A.C., Swetnam, T.W., van der Werf, G.R., Pyne, S.J., 2009. Fire in the earth system. *Science* 324, 481–484. <http://dx.doi.org/10.1126/science.1163886>.
- Bowyer, P., Danson, F.M., 2004. Sensitivity of spectral reflectance to variation in live fuel moisture content at leaf and canopy level. *Remote Sens. Environ.* 92, 297–308. <http://dx.doi.org/10.1016/J.RSE.2004.05.020>.
- Buitrago, M.F., Groen, T.A., Hecker, C.A., Skidmore, A.K., 2016. Changes in thermal infrared spectra of plants caused by temperature and water stress. *ISPRS J. Photogramm. Remote Sens.* 111, 22–31. <http://dx.doi.org/10.1016/j.isprsjprs.2015.11.003>.
- Cao, Z., Wang, Q., 2017. Retrieval of leaf fuel moisture contents from hyperspectral indices developed from dehydration experiments. *Eur. J. Remote Sens.* 50, 18–28. <http://dx.doi.org/10.1080/22797254.2017.1274571>.
- Capitaino, R., Carcaillet, C., 2008. Post-fire Mediterranean vegetation dynamics and diversity: a discussion of succession models. *For. Ecol. Manag.* 255, 431–439. <http://dx.doi.org/10.1016/j.foreco.2007.09.010>.
- Casas, A., Riaño, D., Ustin, S.L., Dennison, P., Salas, J., 2014. Estimation of water-related biochemical and biophysical vegetation properties using multitemporal airborne hyperspectral data and its comparison to MODIS spectral response. *Remote Sens. Environ.* 148, 28–41. <http://dx.doi.org/10.1016/j.rse.2014.03.011>.
- Ceccato, P., Flasse, S., Tarantola, S., Jacquemoud, S., Grégoire, J.-M., 2001. Detecting vegetation leaf water content using reflectance in the optical domain. *Remote Sens. Environ.* 77, 22–33. [http://dx.doi.org/10.1016/S0034-4257\(01\)00191-2](http://dx.doi.org/10.1016/S0034-4257(01)00191-2).
- Chen, M., 2017. Reconstructing Fire Severity and Post-fire Recovery in a Southern California Watershed Using Hyperspectral Imagery and LiDAR. University of California, Santa Barbara.
- Cheng, Y.-B., Zarco-Tejada, P.J., Riaño, D., Rueda, C.A., Ustin, S.L., 2006. Estimating vegetation water content with hyperspectral data for different canopy scenarios: relationships between AVIRIS and MODIS indexes. *Remote Sens. Environ.* 105, 354–366. <http://dx.doi.org/10.1016/J.RSE.2006.07.005>.
- Chu, T., Guo, X., 2013. Remote sensing techniques in monitoring post-fire effects and patterns of forest recovery in boreal forest regions: a review. *Remote Sens.* 6, 470–520. <http://dx.doi.org/10.3390/rs6010470>.
- Chuvieco, E., Aguado, I.A., Cocero, D., Rian, D., Riaño, D., 2003a. Design of an empirical index to estimate fuel moisture content from NOAA-AVHRR images in forest fire danger studies. *Int. J. Remote Sens.* 24, 1621–1637.
- Chuvieco, E., Riaño, D., van Wagtenonk, J., Morsdorf, F., 2003b. Fuel loads and fuel type mapping. In: Chuvieco, E. (Ed.), *Wildland Fire Danger Estimation and Mapping: The Role of Remote Sensing Data*. World Scientific Publishing, Singapore, pp. 119–142.
- Chuvieco, E., Cocero, D., Riaño, D., Martin, P., Martínez-Vega, J., de la Riva, J., Pérez, F., 2004. Combining NDVI and surface temperature for the estimation of live fuel moisture content in forest fire danger rating. *Remote Sens. Environ.* 92, 322–331. <http://dx.doi.org/10.1016/j.rse.2004.01.019>.
- Chuvieco, E., Riaño, D., Danson, F.M., Martin, P., 2006. Use of a radiative transfer model to simulate the postfire spectral response to burn severity. *J. Geophys. Res. Biogeosci.* 111. <http://dx.doi.org/10.1029/2005JG000143>.
- Colgan, M., Baldeck, C., Féret, J.-B., Asner, G., 2012. Mapping savanna tree species at ecosystem scales using support vector machine classification and BRDF correction on airborne hyperspectral and LiDAR data. *Remote Sens.* 4, 3462–3480. <http://dx.doi.org/10.3390/rs4113462>.
- De Santis, A., Chuvieco, E., 2007. Burn severity estimation from remotely sensed data: performance of simulation versus empirical models. *Remote Sens. Environ.* 108, 422–435. <http://dx.doi.org/10.1016/j.rse.2006.11.022>.
- De Santis, A., Chuvieco, E., 2009. GeoCBI: a modified version of the composite burn index for the initial assessment of the short-term burn severity from remotely sensed data. *Remote Sens. Environ.* 113, 554–562. <http://dx.doi.org/10.1016/j.rse.2008.10.011>.
- De Santis, A., Vaughan, P., Chuvieco, E., 2006. Foliage moisture content estimation from one-dimensional and two-dimensional spectroradiometry for fire danger assessment. *J. Geophys. Res. Biogeosci.* 111. <http://dx.doi.org/10.1029/2005JG000149>.
- De Santis, A., Chuvieco, E., Vaughan, P.J., 2009. Short-term assessment of burn severity using the inversion of PROSPECT and GeoSail models. *Remote Sens. Environ.* 113, 126–136. <http://dx.doi.org/10.1016/J.RSE.2008.08.008>.
- De Santis, A., Asner, G.P., Vaughan, P.J., Knapp, D.E., 2010. Mapping burn severity and burning efficiency in California using simulation models and Landsat imagery. *Remote Sens. Environ.* 114, 1535–1545. <http://dx.doi.org/10.1016/j.rse.2010.02.008>.
- Dennison, P.E., 2006. Fire detection in imaging spectrometer data using atmospheric carbon dioxide absorption. *Int. J. Remote Sens.* 27, 3049–3055. <http://dx.doi.org/10.1080/01431160600660871>.
- Dennison, P.E., Matheson, D.S., 2011. Comparison of fire temperature and fractional area modeled from SWIR, MIR, and TIR multispectral and SWIR hyperspectral airborne data. *Remote Sens. Environ.* 115, 876–886. <http://dx.doi.org/10.1016/j.rse.2010.11.015>.
- Dennison, P.E., Roberts, D.A., 2009. Daytime fire detection using airborne hyperspectral data. *Remote Sens. Environ.* 113, 1646–1657. <http://dx.doi.org/10.1016/j.rse.2009.03.010>.
- Dennison, P.E., Roberts, D.A., Thorgusen, S.R., Regelbrugge, J.C., Weise, D., Lee, C., 2003. Modeling seasonal changes in live fuel moisture and equivalent water thickness using a cumulative water balance index. *Remote Sens. Environ.* 88, 442–452. <http://dx.doi.org/10.1016/J.RSE.2003.08.015>.
- Dennison, P., Charoensiri, K., Roberts, D., Peterson, S., Green, R., 2006. Wildfire temperature and land cover modeling using hyperspectral data. *Remote Sens. Environ.* 100, 212–222. <http://dx.doi.org/10.1016/j.rse.2005.10.007>.
- Dennison, P.E., Brewer, S.C., Arnold, J.D., Moritz, M.A., 2014. Large wildfire trends in the western United States, 1984–2011. *Geophys. Res. Lett.* 41, 2928–2933. <http://dx.doi.org/10.1002/2014GL059576>.
- Díaz-Delgado, R., Lloret, F., Pons, X., 2003. Influence of fire severity on plant regeneration by means of remote sensing imagery. *Int. J. Remote Sens.* 24, 1751–1763. <http://dx.doi.org/10.1080/01431160210144732>.
- Diner, D.J., Xu, F., Garay, M.J., Martonchik, J.V., Rheingans, B.E., Geier, S., Davis, A., Hancock, B.R., Jovanovic, V.M., Bull, M.A., Capraro, K., Chipman, R.A., McClain, S.C., 2013. The airborne multiangle spectropolarimetric imager (AirMSPi): a new tool for aerosol and cloud remote sensing. *Atmos. Meas. Tech.* 6, 2007–2025. <http://dx.doi.org/10.5194/amt-6-2007-2013>.
- Dudley, K., Dennison, P.E., Roth, K., Roberts, D.A., Coates, A., 2015. A multi-temporal spectral library approach for mapping vegetation species across spatial and temporal phenological gradients. *Remote Sens. Environ.* 167, 121–134. <http://dx.doi.org/10.1016/J.RSE.2015.05.004>.
- Eckmann, T., Roberts, D., Still, C., 2008. Using multiple endmember spectral mixture analysis to retrieve subpixel fire properties from MODIS. *Remote Sens. Environ.* 112, 3773–3783. <http://dx.doi.org/10.1016/j.rse.2008.05.008>.
- Eckmann, T.C., Roberts, D.A., Still, C.J., 2009. Estimating subpixel fire sizes and temperatures from ASTER using multiple endmember spectral mixture analysis. *Int. J. Remote Sens.* 30, 5851–5864. <http://dx.doi.org/10.1080/01431160902748531>.
- Eidenshink, J., Schwind, B., Brewer, K., Zhu, Z., Quayle, B., Howard, S., 2007. A project for monitoring trends in burn severity. *Fire Ecol.* 3, 3–21.
- Feingersh, T., Ben Dor, E., 2016. SHALOM - a commercial hyperspectral space mission. In: Qian, S. (Ed.), *Optical Payloads for Space Missions*. John Wiley & Sons, Pondicherry, India, pp. 247–263.
- Fernandez-Manso, O., Quintano, C., Fernandez-Manso, A., 2009. Combining spectral mixture analysis and object-based classification for fire severity mapping. *Investig. Agrar. y Recur. For.* 18, 296–313.
- Forkel, M., Thonicke, K., Beer, C., Cramer, W., Bartalev, S., Schullius, C., 2012. Extreme fire events are related to previous-year surface moisture conditions in permafrost-underrlain larch forests of Siberia. *Environ. Res. Lett.* 7, 044021. <http://dx.doi.org/10.1088/1748-9326/7/4/044021>.
- French, N.H.F., Kasischke, E.S., Hall, R.J., Murphy, K.A., Verbyla, D.L., Hoy, E.E., Allen, J.L., 2008. Using Landsat data to assess fire and burn severity in the North American boreal forest region: an overview and summary of results. *Int. J. Wildland Fire* 17, 443. <http://dx.doi.org/10.1071/WF08007>.
- Friedl, M., McIver, D., Hodges, J.C., Zhang, X., Muchoney, D., Strahler, A., Woodcock, C., Gopal, S., Schneider, A., Cooper, A., Baccini, A., Gao, F., Schaaf, C., 2002. Global land cover mapping from MODIS: algorithms and early results. *Remote Sens. Environ.* 83, 287–302. [http://dx.doi.org/10.1016/S0034-4257\(02\)00078-0](http://dx.doi.org/10.1016/S0034-4257(02)00078-0).
- Gamon, J.A., Serrano, L., Surfus, J.S., 1997. The photochemical reflectance index: an optical indicator of photosynthetic radiation use efficiency across species, functional types, and nutrient levels. *Oecologia* 112, 492–501. <http://dx.doi.org/10.1007/s004420050337>.
- Gao, B.-C., 1995. A normalized difference water index for remote sensing of vegetation liquid water from space. In: *Proc. SPIE 2480, Imaging Spectrometry*, 225 (June 12, 1995). Orlando, Florida, USA, pp. 225–236. <http://dx.doi.org/10.1117/12.210877>.
- Giglio, L., Kendall, J.D., 2001. Application of the Dozier retrieval to wildfire characterization: a sensitivity analysis. *Remote Sens. Environ.* 77, 34–49. [http://dx.doi.org/10.1016/S0034-4257\(01\)00192-4](http://dx.doi.org/10.1016/S0034-4257(01)00192-4).
- Giglio, L., Schroeder, W., 2014. A global feasibility assessment of the bi-spectral fire temperature and area retrieval using MODIS data. *Remote Sens. Environ.* 152, 166–173. <http://dx.doi.org/10.1016/j.rse.2014.06.010>.
- Giglio, L., Desloires, J., Justice, C.O., Kaufman, Y.J., 2003. An enhanced contextual fire detection algorithm for MODIS. *Remote Sens. Environ.* 87, 273–282. [http://dx.doi.org/10.1016/S0034-4257\(03\)00184-6](http://dx.doi.org/10.1016/S0034-4257(03)00184-6).
- Giglio, L., Loboda, T., Roy, D.P., Quayle, B., Justice, C.O., 2009. An active-fire based burned area mapping algorithm for the MODIS sensor. *Remote Sens. Environ.* 113, 408–420. <http://dx.doi.org/10.1016/j.rse.2008.10.006>.
- Gillet, N.P., Weaver, A.J., Zwiers, F.W., Flannigan, M.D., 2004. Detecting the effect of climate change on Canadian forest fires. *Geophys. Res. Lett.* 31, L18211. <http://dx.doi.org/10.1029/2004GL020876>.
- Gitas, I.Z., Polychronaki, A., Katagis, T., Mallinis, G., 2008. Contribution of remote sensing to disaster management activities: a case study of the large fires in the Peloponnese, Greece. *Int. J. Remote Sens.* 29, 1847–1853. <http://dx.doi.org/10.1080/01431160701874553>.
- Gitas, I., Mitri, G., Veraverbeke, S., Polychronaki, A., 2012. Advances in remote sensing of post-fire vegetation recovery monitoring—a review. *Remote Sens. Biomass Princ.*

- Appl. 322.
- Goetz, S.J., Fiske, G.J., Bunn, A.G., 2006. Using satellite time-series data sets to analyze fire disturbance and forest recovery across Canada. *Remote Sens. Environ.* 101, 352–365. <http://dx.doi.org/10.1016/j.rse.2006.01.011>.
- Gouveia, C., DaCamara, C.C., Trigo, R.M., 2010. Post-fire vegetation recovery in Portugal based on spot/vegetation data. *Nat. Hazards Earth Syst. Sci.* 10, 673–684. <http://dx.doi.org/10.5194/nhess-10-673-2010>.
- Green, R.O., Eastwood, M.L., Sarture, C.M., Chrien, T.G., Aronsson, M., Chippendale, B.J., Faust, J.A., Pavri, B.E., Chovit, C.J., Solis, M., Olah, M.R., Williams, O., 1998. Imaging spectroscopy and the airborne visible/infrared imaging spectrometer (AVIRIS). *Remote Sens. Environ.* 65, 227–248. [http://dx.doi.org/10.1016/S0034-4257\(98\)00064-9](http://dx.doi.org/10.1016/S0034-4257(98)00064-9).
- Hansen, M.C., Reed, B., 2000. A comparison of the IGBP DISCover and University of Maryland 1 km global land cover products. *Int. J. Remote Sens.* 21, 1365–1373. <http://dx.doi.org/10.1080/014311600210218>.
- Hegg, D.A., Radke, L.F., Hobbs, P.V., Riggan, P.J., 1988. Ammonia emissions from biomass burning. *Geophys. Res. Lett.* 15, 335–337. <http://dx.doi.org/10.1029/GL015i004p00335>.
- Hook, S.J., Myers, J.J., Thome, K.J., Fitzgerald, M., Kahle, A.B., 2001. The MODIS/ASTER airborne simulator (MASTER) — a new instrument for earth science studies. *Remote Sens. Environ.* 76, 93–102. [http://dx.doi.org/10.1016/S0034-4257\(00\)00195-4](http://dx.doi.org/10.1016/S0034-4257(00)00195-4).
- Huesca, M., Merino-de-Miguel, S., González-Alonso, F., Martínez, S., Miguel Cuevas, J., Calle, A., 2013. Using AHS hyper-spectral images to study forest vegetation recovery after a fire. *Int. J. Remote Sens.* 34, 4025–4048. <http://dx.doi.org/10.1080/01431161.2013.772313>.
- Hulley, G.C., Duren, R.M., Hopkins, F.M., Hook, S.J., Vance, N., Guillevic, P., Johnson, W.R., Eng, B.T., Mihaly, J.M., Jovanovic, V.M., Chazanoff, S.L., Staniszewski, Z.K., Kuai, L., Worden, J., Frankenberg, C., Rivera, G., Aubrey, A.D., Miller, C.E., Malakar, N.K., Sánchez Tomás, J.M., Holmes, K.T., 2016. High spatial resolution imaging of methane and other trace gases with the airborne hyperspectral thermal emission spectrometer (HyTES). *Atmos. Meas. Tech.* 9, 2393–2408. <http://dx.doi.org/10.5194/amt-9-2393-2016>.
- Itten, K.I., Dell'Endice, F., Hueni, A., Kneubühler, M., Schläpfer, D., Odermatt, D., Seidel, F., Huber, S., Schopfer, J., Kellenberger, T., Bühler, Y., D'Odorico, P., Nieke, J., Alberti, E., Meuleman, K., 2008. APEX - the hyperspectral ESA airborne prism experiment. *Sensors* 8, 6235–6259. <http://dx.doi.org/10.3390/s8106235>.
- Iwasaki, A., Ohgi, N., Tani, J., Kawashima, T., Inada, H., 2011. Hyperspectral imager suite (HISUI) - Japanese hyper-multi spectral radiometer. In: 2011 IEEE International Geoscience and Remote Sensing Symposium. IEEE, pp. 1025–1028. <http://dx.doi.org/10.1109/IGARSS.2011.6049308>.
- Jackson, T.J., Chen, D., Cosh, M., Li, F., Anderson, M., Walthall, C., Doriaswamy, P., Hunt, E.R., 2004. Vegetation water content mapping using Landsat data derived normalized difference water index for corn and soybeans. *Remote Sens. Environ.* 92, 475–482. <http://dx.doi.org/10.1016/j.rse.2003.10.021>.
- Jain, T., Graham, R., Pilliod, D., 2004. Tongue-tied: confused meanings for common fire terminology can lead to fuels mismanagement. *Wildfire July/August*, 22–26.
- Jia, G.J., Burke, I.C., Goetz, A.F.H., Kaufmann, M.R., Kindel, B.C., 2006a. Assessing spatial patterns of forest fuel using AVIRIS data. *Remote Sens. Environ.* 102, 318–327. <http://dx.doi.org/10.1016/j.rse.2006.02.025>.
- Jia, G.J., Burke, I.C., Kaufmann, M.R., Goetz, A.F.H., Kindel, B.C., Pu, Y., 2006b. Estimates of forest canopy fuel attributes using hyperspectral data. *For. Ecol. Manag.* 229, 27–38. <http://dx.doi.org/10.1016/j.foreco.2006.03.021>.
- Johnstone, J.F., Kasischke, E.S., 2005. Stand-level effects of soil burn severity on postfire regeneration in a recently burned black spruce forest. *Can. J. For. Res.* 35, 2151–2163. <http://dx.doi.org/10.1139/x05-087>.
- Jurdao, S., Yebra, M., Guerschman, J.P., Chuvieco, E., 2013. Regional estimation of woodland moisture content by inverting radiative transfer models. *Remote Sens. Environ.* 132, 59–70. <http://dx.doi.org/10.1016/j.rse.2013.01.004>.
- Kalashnikova, O.V., Garay, M.J., Bates, K.H., Kenseth, C.M., Kong, W., Cappa, C.D., Lyapunin, A.L., Jonsson, H.H., Seidel, F.C., Xu, F., Diner, D.J., Seinfeld, J.H., 2018. Photopolarimetric sensitivity to black carbon content of wildfire smoke: results from the 2016 ImpACT-PM field campaign. *J. Geophys. Res. Atmos.* <http://dx.doi.org/10.1029/2017JD028032>.
- Katagis, T., Gitas, I.Z., Toukiloglou, P., Veraverbeke, S., Goossens, R., 2014. Trend analysis of medium- and coarse-resolution time series image data for burned area mapping in a Mediterranean ecosystem. *Int. J. Wildland Fire* 23, 668–677.
- Keeley, J.E., 2009. Fire intensity, fire severity and burn severity: a brief review and suggested usage. *Int. J. Wildland Fire* 18, 116. <http://dx.doi.org/10.1071/WF07049>.
- Key, C.H., Benson, N.C., 2006. Landscape assessment: ground measure of severity; the Composite Burn Index, and remote sensing of severity, the Normalized Burn Index. In: Lutes, D., Keane, R., Caratti, J., Key, C., Benson, N., Sutherland, S., Grangi, L. (Eds.), FIREMON: Fire Effects Monitoring and Inventory System. USDA Forest Service, pp. 1–51.
- Kokaly, R.F., Rockwell, B.W., Haire, S.L., King, T.V.V., 2007. Characterization of post-fire surface cover, soils, and burn severity at the Cerro Grande Fire, New Mexico, using hyperspectral and multispectral remote sensing. *Remote Sens. Environ.* 106, 305–325. <http://dx.doi.org/10.1016/j.rse.2006.08.006>.
- Koutsias, N., Karteris, M., 2000. Burned area mapping using logistic regression modeling of a single post-fire Landsat-5 Thematic Mapper image. *Int. J. Remote Sens.* 21, 673–687. <http://dx.doi.org/10.1080/014311600210506>.
- Kuai, L., Worden, J.R., Li, K.-F., Hulley, G.C., Hopkins, F.M., Miller, C.E., Hook, S.J., Duren, R.M., Aubrey, A.D., 2016. Characterization of anthropogenic methane plumes with the hyperspectral thermal emission spectrometer (HyTES): a retrieval method and error analysis. *Atmos. Meas. Tech.* 9, 3165–3173. <http://dx.doi.org/10.5194/amt-9-3165-2016>.
- Labate, D., Ceccherini, M., Cisbani, A., De Cosmo, V., Galeazzi, C., Giunti, L., Melozzi, M., Pieraccini, S., Stagi, M., 2009. The PRISMA payload optomechanical design, a high performance instrument for a new hyperspectral mission. *Acta Astronaut.* 65, 1429–1436. <http://dx.doi.org/10.1016/j.actaastro.2009.03.077>.
- Lee, C.M., Cable, M.L., Hook, S.J., Green, R.O., Ustin, S.L., Mandl, D.J., Middleton, E.M., 2015. An introduction to the NASA Hyperspectral InfraRed Imager (HyspIRI) mission and preparatory activities. *Remote Sens. Environ.* 167, 6–19. <http://dx.doi.org/10.1016/j.rse.2015.06.012>.
- Lentile, L.B., Holden, Z.A., Smith, A.M.S., Falkowski, M.J., Hudak, A.T., Morgan, P., Lewis, S.A., Gessler, P.E., Benson, N.C., 2006. Remote sensing techniques to assess active fire characteristics and post-fire effects. *Int. J. Wildland Fire* 15, 319. <http://dx.doi.org/10.1071/WF05097>.
- Leon, J.R.R., van Leeuwen, W.J.D., Casady, G.M., 2012. Using MODIS-NDVI for the modeling of post-wildfire vegetation response as a function of environmental conditions and pre-fire restoration treatments. *Remote Sens.* 4, 598–621. <http://dx.doi.org/10.3390/rs4030598>.
- Levick, S.R., Baldeck, C.A., Asner, G.P., 2015. Demographic legacies of fire history in an African savanna. *Funct. Ecol.* 29, 131–139. <http://dx.doi.org/10.1111/1365-2435.12306>.
- Lewis, S.A., Lentile, L.B., Hudak, A.T., Robichaud, P.R., Morgan, P., Bobbitt, M.J., 2007. Mapping ground cover using hyperspectral remote sensing after the 2003 Simi and old wildfires in Southern California. *Fire Ecol.* 3, 109–128. <http://dx.doi.org/10.4996/fireecology.0301109>.
- Lewis, S.A., Robichaud, P.R., Frazier, B.E., Wu, J.Q., Laes, D.Y.M., 2008. Using hyperspectral imagery to predict post-wildfire soil water repellency. *Geomorphology* 95, 192–205. <http://dx.doi.org/10.1016/j.geomorph.2007.06.002>.
- Lewis, S.A., Hudak, A.T., Ottmar, R.D., Robichaud, P.R., Lentile, L.B., Hood, S.M., Cronan, J.B., Morgan, P., 2011. Using hyperspectral imagery to estimate forest floor consumption from wildfire in boreal forests of Alaska, USA. *Int. J. Wildland Fire* 20, 255. <http://dx.doi.org/10.1071/WF09081>.
- Lewis, S.A., Hudak, A.T., Robichaud, P.R., Morgan, P., Satterberg, K.L., Strand, E.K., Smith, A.M.S., Zamudio, J.A., Lentile, L.B., 2017. Indicators of burn severity at extended temporal scales: a decade of ecosystem response in mixed-conifer forests of western Montana. *Int. J. Wildland Fire* 26, 755. <http://dx.doi.org/10.1071/WF17019>.
- Liu, W.T., Kogan, F.N., 1996. Monitoring regional drought using the vegetation condition index. *Int. J. Remote Sens.* 17, 2761–2782. <http://dx.doi.org/10.1080/01431169608949106>.
- Liu, S., Aiken, A.C., Arata, C., Dubey, M.K., Stockwell, C.E., Yokelson, R.J., Stone, E.A., Jayarathne, T., Robinson, A.L., DeMott, P.J., Kreidenweis, S.M., 2014. Aerosol single scattering albedo dependence on biomass combustion efficiency: laboratory and field studies. *Geophys. Res. Lett.* 41, 742–748. <http://dx.doi.org/10.1002/2013GL058392>.
- López García, M.J., Caselles, V., 1991. Mapping burns and natural reforestation using thematic mapper data. *Geocarto Int.* 6, 31–37. <http://dx.doi.org/10.1080/10106049109354290>.
- Loveland, T.R., Reed, B.C., Brown, J.F., Ohlen, D.O., Zhu, Z., Yang, L., Merchant, J.W., 2000. Development of a global land cover characteristics database and IGBP DISCover from 1 km AVHRR data. *Int. J. Remote Sens.* 21, 1303–1330. <http://dx.doi.org/10.1080/014311600210191>.
- Marino, E., Ranz, P., Tomé, J.L., Noriega, M.A., Esteban, J., Madrigal, J., 2016. Generation of high-resolution fuel model maps from discrete airborne laser scanner and Landsat-8 OLI: a low-cost and highly updated methodology for large areas. *Remote Sens. Environ.* 187, 267–280. <http://dx.doi.org/10.1016/j.rse.2016.10.020>.
- Matheson, D.S., Dennison, P.E., 2012. Evaluating the effects of spatial resolution on hyperspectral fire detection and temperature retrieval. *Remote Sens. Environ.* 124, 780–792. <http://dx.doi.org/10.1016/j.rse.2012.06.026>.
- Matson, M., Holben, B., 1987. Satellite detection of tropical burning in Brazil. *Int. J. Remote Sens.* 8, 509–516. <http://dx.doi.org/10.1080/01431168708948657>.
- McElhinny, C., Gibbons, P., Brack, C., Bauhus, J., 2005. Forest and woodland stand structural complexity: its definition and measurement. *For. Ecol. Manag.* 218, 1–24. <http://dx.doi.org/10.1016/j.foreco.2005.08.034>.
- Meerdink, S.K., Roberts, D.A., King, J.Y., Roth, K.L., Dennison, P.E., Amaral, C.H., Hook, S.J., 2016. Linking seasonal foliar traits to VSWIR-TIR spectroscopy across California ecosystems. *Remote Sens. Environ.* 186, 322–338. <http://dx.doi.org/10.1016/j.rse.2016.08.003>.
- Meng, R., Wu, J., Schwager, K., Zhao, F., Dennison, P., Cook, B., Brewster, K., Green, T., Serbin, S., 2017. Using high spatial resolution satellite imagery to map forest burn severity across spatial scales in a pine barrens ecosystem. *Remote Sens. Environ.* 191, 95–109.
- Meng, R., Wu, J., Zhao, F., Cook, B.D., Hanavan, R.P., Serbin, S.P., 2018. Measuring short-term post-fire forest recovery across a burn severity gradient in a mixed pine-oak forest using multi-sensor remote sensing techniques. *Remote Sens. Environ.* 210, 282–296. <http://dx.doi.org/10.1016/j.rse.2018.03.019>.
- Merrill, D.F., Alexander, M.E., 1987. Glossary of Forest Fire Management Terms.
- Mitri, Gitas, I., 2006. Fire type mapping using object-based classification of Ikonos imagery. *Int. J. Wildland Fire* 15, 457. <http://dx.doi.org/10.1071/WF05085>.
- Mitri, G.H., Gitas, I.Z., 2010. Mapping postfire vegetation recovery using EO-1 hyperion imagery. *IEEE Trans. Geosci. Remote Sens.* 48, 1613–1618. <http://dx.doi.org/10.1109/TGRS.2009.2031557>.
- Mitri, G.H., Gitas, I.Z., 2013. Mapping post-fire forest regeneration and vegetation recovery using a combination of very high spatial resolution and hyperspectral satellite imagery. *Int. J. Appl. Earth Obs. Geoinf.* 20, 60–66. <http://dx.doi.org/10.1016/j.jag.2011.09.001>.
- Moreira, F., Catry, F., Duarte, I., Acácio, V., Silva, J.S., 2009. A conceptual model of sprouting responses in relation to fire damage: an example with cork oak (*Quercus suber* L.) trees in Southern Portugal. In: *Forest Ecology: Recent Advances in Plant*

- Ecology, pp. 77–85. <http://dx.doi.org/10.1007/978-90-481-2795-5.7>.
- Morgan, P., Keane, R.E., Dillon, G.K., Jain, T.B., Hudak, A.T., Karau, E.C., Sikkink, P.G., Holden, Z.A., Strand, E.K., 2014. Challenges of assessing fire and burn severity using field measures, remote sensing and modelling. *Int. J. Wildland Fire* 23, 1045. <http://dx.doi.org/10.1071/WF13058>.
- National Academies of Sciences, E. and M., 2018. *Thriving on our Changing Planet*. National Academies Press, Washington, D.C. <http://dx.doi.org/10.17226/24938>.
- Neinavaz, E., Skidmore, A.K., Darvishzadeh, R., Groen, T.A., 2017. Retrieving vegetation canopy water content from hyperspectral thermal measurements. *Agric. For. Meteorol.* 247, 365–375. <http://dx.doi.org/10.1016/J.AGRFORMET.2017.08.020>.
- Nelson, K.J., Connot, J., Peterson, B., Martin, C., 2013. The LANDFIRE refresh strategy: updating the national dataset. *Fire Ecol.* 9, 80–101. <http://dx.doi.org/10.4996/fireecology.090280>.
- Numata, I., Cochrane, M.A., Galvão, L.S., Numata, I., Cochrane, M.A., Galvão, L.S., 2011. Analyzing the impacts of frequency and severity of forest fire on the recovery of disturbed forest using Landsat time series and EO-1 hyperion in the southern Brazilian Amazon. *Earth Interact.* 15, 1–17. <http://dx.doi.org/10.1175/2010EI372.1>.
- Oertel, D., Zhukov, B., Thamm, H.-P., Roehrig, J., Orthmann, B., 2004. Space-borne high resolution fire remote sensing in Benin, West Africa. *Int. J. Remote Sens.* 25, 2209–2216. <http://dx.doi.org/10.1080/01431160320001647741>.
- Parsons, A., Robichaud, P.R., Lewis, S.A., Napper, C., Clark, J.T., 2010. Field guide for mapping post-fire soil burn severity. In: Gen. Tech. Rep. RMRS-GTR-243. U.S. Department of Agriculture, Forest Service, Rocky Mountain Research Station, Fort Collins, CO 49 p. <https://doi.org/10.2737/RMRS-GTR-243>.
- Pausas, J., Fernández-Muñoz, S., 2012. Fire regime changes in the Western Mediterranean Basin: from fuel-limited to drought-driven fire regime. *Clim. Chang.* 110, 215–226. <http://dx.doi.org/10.1007/s10584-011-0060-6>.
- Pearlman, J.S., Barry, P.S., Segal, C.C., Shepanski, J., Beiso, D., Carman, S.L., 2003. Hyperion, a space-based imaging spectrometer. *IEEE Trans. Geosci. Remote Sens.* 41, 1160–1173. <http://dx.doi.org/10.1109/TGRS.2003.815018>.
- Pereira, J.M.C., 2003. Remote sensing of burned areas in tropical savannas. *Int. J. Wildland Fire* 12, 259. <http://dx.doi.org/10.1071/WF03028>.
- Pérez-Cabello, F., Echeverría, M.T., Ibarra, P., de la Riva, J., 2009. Effects of fire on vegetation, soil and hydrogeomorphological behavior in Mediterranean ecosystems. In: *Earth Observation of Wildland Fires in Mediterranean Ecosystems*. Springer Berlin Heidelberg, Berlin, Heidelberg, pp. 111–128. http://dx.doi.org/10.1007/978-3-642-01754-4_9.
- Peterson, S.H., Franklin, J., Roberts, D.A., van Wagtenonk, J.W., 2013. Mapping fuels in Yosemite National Park. *Can. J. For. Res.* 43, 7–17. <http://dx.doi.org/10.1139/cjfr-2012-0213>.
- Pickett, B.M., Isackson, C., Wunder, R., Fletcher, T.H., Butler, B.W., Weise, D.R., 2010. Experimental measurements during combustion of moist individual foliage samples. *Int. J. Wildland Fire* 19, 153. <http://dx.doi.org/10.1071/WF07121>.
- Pinty, B., Verstraete, M.M., 1992. GEMI: a non-linear index to monitor global vegetation from satellites. *Vegetatio* 101, 15–20. <http://dx.doi.org/10.1007/BF00031911>.
- Qiu, H., Gamon, J.A., Roberts, D.A., Luna, M., 1998. Monitoring postfire succession in the Santa Monica mountains using hyperspectral imagery. In: Green, R.O., Tong, Q. (Eds.), *International Society for Optics and Photonics*, pp. 201–208. <http://dx.doi.org/10.1117/12.317812>.
- Quintano, C., Fernández-Manso, A., Roberts, D.A., 2013. Multiple endmember spectral mixture analysis (MESMA) to map burn severity levels from Landsat images in Mediterranean countries. *Remote Sens. Environ.* 136, 76–88. <http://dx.doi.org/10.1016/j.rse.2013.04.017>.
- Realmuto, V.J., Dennison, P.E., Foote, M., Ramsey, M.S., Wooster, M.J., Wright, R., 2015. Specifying the saturation temperature for the HypsIRI 4- μ m channel. *Remote Sens. Environ.* 167, 40–52. <http://dx.doi.org/10.1016/j.rse.2015.04.028>.
- Reid, J.S., Koppmann, R., Eck, T.F., Eleuterio, D.P., 2005. A review of biomass burning emissions part II: intensive physical properties of biomass burning particles. *Atmos. Chem. Phys.* 5, 799–825.
- Riaño, D., Chuvieco, E., Ustin, S., Zomer, R., Dennison, P., Roberts, D., Salas, J., 2002. Assessment of vegetation regeneration after fire through multitemporal analysis of AVIRIS images in the Santa Monica Mountains. *Remote Sens. Environ.* 79, 60–71. [http://dx.doi.org/10.1016/S0034-4257\(01\)00239-5](http://dx.doi.org/10.1016/S0034-4257(01)00239-5).
- Riaño, D., Meier, E., Allgoewer, B., Chuvieco, E., Ustin, S., 2003. Modeling airborne laser scanning data for the spatial generation of critical forest parameters in fire behavior modeling. *Remote Sens. Environ.* 86, 177–186. [http://dx.doi.org/10.1016/S0034-4257\(03\)00098-1](http://dx.doi.org/10.1016/S0034-4257(03)00098-1).
- Riano, D., Vaughan, P., Chuvieco, E., Zarco-Tejada, P.J., Ustin, S.L., 2005. Estimation of fuel moisture content by inversion of radiative transfer models to simulate equivalent water thickness and dry matter content: analysis at leaf and canopy level. *IEEE Trans. Geosci. Remote Sens.* 43, 819–826. <http://dx.doi.org/10.1109/TGRS.2005.843316>.
- Riggan, P.J., Tissell, R.G., Lockwood, R.N., Brass, J.A., Pereira, J.A.R., Miranda, H.S., Miranda, A.C., Campos, T., Higgins, R., 2004. Remote measurement of energy and carbon flux from wildfires in Brazil. *Ecol. Appl.* 14, 855–872. <http://dx.doi.org/10.1890/02-5162>.
- Roberts, G.J., Wooster, M.J., 2008. Fire detection and fire characterization over Africa using Meteosat SEVIRI. *IEEE Trans. Geosci. Remote Sens.* 46, 1200–1218. <http://dx.doi.org/10.1109/TGRS.2008.915751>.
- Roberts, D.A., Smith, M.O., Adams, J.B., 1993. Green vegetation, nonphotosynthetic vegetation, and soils in AVIRIS data. *Remote Sens. Environ.* 44, 255–269. [http://dx.doi.org/10.1016/0034-4257\(93\)90020-X](http://dx.doi.org/10.1016/0034-4257(93)90020-X).
- Roberts, D.A., Gardner, M., Church, R., Ustin, S., Scheer, G., Green, R.O., 1998. Mapping chaparral in the Santa Monica mountains using multiple endmember spectral mixture models. *Remote Sens. Environ.* 65, 267–279. [http://dx.doi.org/10.1016/S0034-4257\(98\)00037-6](http://dx.doi.org/10.1016/S0034-4257(98)00037-6).
- Roberts, D.A., Dennison, P.E., Gardner, M.E., Hetzel, Y., Ustin, S.L., Lee, C.T., 2003. Evaluation of the potential of Hyperion for fire danger assessment by comparison to the airborne visible/infrared imaging spectrometer. *IEEE Trans. Geosci. Remote Sens.* 41, 1297–1310. <http://dx.doi.org/10.1109/TGRS.2003.812904>.
- Roberts, D.A., Dennison, P.E., Peterson, S., Sweeney, S., Rechel, J., 2006. Evaluation of airborne visible/infrared imaging spectrometer (AVIRIS) and moderate resolution imaging spectrometer (MODIS) measures of live fuel moisture and fuel condition in a shrubland ecosystem in southern California. *J. Geophys. Res. Biogeosci.* 111. <http://dx.doi.org/10.1029/2005JG000113>.
- Robichaud, P.R., Ashmun, L.E., 2013. Tools to aid post-wildfire assessment and erosion-mitigation treatment decisions. *Int. J. Wildland Fire* 22, 95. <http://dx.doi.org/10.1071/WF11162>.
- Robichaud, P.R., Lewis, S.A., Laes, D.Y.M., Hudak, A.T., Kokaly, R.F., Zamudio, J.A., 2007. Postfire soil burn severity mapping with hyperspectral image unmixing. *Remote Sens. Environ.* 108, 467–480. <http://dx.doi.org/10.1016/j.rse.2006.11.027>.
- Rogers, B.M., Veraverbeke, S., Azzari, G., Czimczik, C.I., Holden, S.R., Mouteva, G.O., Sedano, F., Treseder, K.K., Randerson, J.T., 2014. Quantifying fire-wide carbon emissions in interior Alaska using field measurements and Landsat imagery. *J. Geophys. Res.* 119, 1608–1629.
- Rogge, D.M., Rivard, B., Zhang, J., Feng, J., 2006. Iterative spectral unmixing for optimization per-pixel endmember sets. *IEEE Trans. Geosci. Remote Sens.* 44, 3725–3736. <http://dx.doi.org/10.1109/TGRS.2006.881123>.
- Rollins, M.G.B.C., Frame, C.K., Keane, R.E., Zhu, Z., Menakis, J.P.B., Caratti, J.F., Holsinger, L., Parsons, R.F., Karau, E., Long, J.L.E.G., Miller, M.H., Fresco, T.S.J., Vogelmann, J.L., Ohlen, D., Kost, J.L., Chen, X.L., Tolk, B.L., Long, D., Losensky, B.J., Bedunah, D., Pratt, S., Steele, B., Eidenshink, J., 2006. The LANDFIRE prototype project: nationally consistent and locally relevant geospatial data for wildland fire management. In: *USDA For. Serv. - Gen. Tech. Rep. RMRS-GTR*, pp. 1–418.
- Roth, K.L., Dennison, P.E., Roberts, D.A., 2012. Comparing endmember selection techniques for accurate mapping of plant species and land cover using imaging spectrometer data. *Remote Sens. Environ.* 127, 139–152. <http://dx.doi.org/10.1016/j.rse.2012.08.030>.
- Rothman, L.S., Gordon, I.E., Babikov, Y., Barbe, A., Chris Benner, D., Bernath, P.F., Birk, M., Bizzocchi, L., Boudon, V., Brown, L.R., Campargue, A., Chance, K., Cohen, E.A., Coudert, L.H., Devi, V.M., Drouin, B.J., Fayt, A., Flaud, J.-M., Gamache, R.R., Harrison, J.J., Hartmann, J.-M., Hill, C., Hodges, J.T., Jacquemart, D., Jolly, A., Lamouroux, J., Le Roy, R.J., Li, G., Long, D.A., Lyulin, O.M., Mackie, C.J., Massie, S.T., Mikhailenko, S., Müller, H.S.P., Naumenko, O.V., Nikitin, A.V., Orphal, J., Perevalov, V., Perrin, A., Polovtseva, E.R., Richard, C., Smith, M.A.H., Starikova, E., Sung, K., Tashkun, S., Tennyson, J., Toon, G.C., Tyuterev, V.G., Wagner, G., 2013. The HITRAN2012 molecular spectroscopic database. *J. Quant. Spectrosc. Radiat. Transf.* 130, 4–50. <http://dx.doi.org/10.1016/j.jqsrt.2013.07.002>.
- Roy, D.P., Jin, Y., Lewis, P.E., Justice, C.O., 2005. Prototyping a global algorithm for systematic fire-affected area mapping using MODIS time series data. *Remote Sens. Environ.* 97, 137–162. <http://dx.doi.org/10.1016/j.rse.2005.04.007>.
- Roy, D.P., Boschetti, L., Trigg, S.N., 2006. Remote sensing of fire severity: assessing the performance of the normalized burn ratio. *IEEE Geosci. Remote Sens. Lett.* 3, 112–116. <http://dx.doi.org/10.1109/LGRS.2005.858485>.
- Ryan, K.C., Opperman, T.S., 2013. LANDFIRE – a national vegetation/fuels data base for use in fuels treatment, restoration, and suppression planning. *For. Ecol. Manag.* 294, 208–216. <http://dx.doi.org/10.1016/j.foreco.2012.11.003>.
- Schaepman, M.E., Ustin, S.L., Plaza, A.J., Painter, T.H., Verrelst, J., Liang, S., 2009. Earth system science related imaging spectroscopy—an assessment. *Remote Sens. Environ.* 113, S123–S137. <http://dx.doi.org/10.1016/j.rse.2009.03.001>.
- Schepers, L., Haest, B., Veraverbeke, S., Spanhove, T., Vanden Borre, J., Goossens, R., 2014. Burned area detection and burn severity assessment of a heathland fire in Belgium using airborne imaging spectroscopy (APEX). *Remote Sens.* 6, 1803–1826. <http://dx.doi.org/10.3390/rs6031803>.
- Schimel, D.S., Asner, G.P., Moorcroft, P., 2013. Observing changing ecological diversity in the Anthropocene. *Front. Ecol. Environ.* 11, 129–137. <http://dx.doi.org/10.1890/120111>.
- Schlerf, M., Atzberger, C., Hill, J., 2005. Remote sensing of forest biophysical variables using HyMap imaging spectrometer data. *Remote Sens. Environ.* 95, 177–194. <http://dx.doi.org/10.1016/J.RSE.2004.12.016>.
- Schroeder, W., Oliva, P., Giglio, L., Csiszar, I.A., 2014. The new VIIRS 375 m active fire detection data product: algorithm description and initial assessment. *Remote Sens. Environ.* 143, 85–96. <http://dx.doi.org/10.1016/j.rse.2013.12.008>.
- Serrano, L., Ustin, S.L., Roberts, D.A., Gamon, J.A., Peñuelas, J., 2000. Deriving water content of chaparral vegetation from AVIRIS data. *Remote Sens. Environ.* 74, 570–581. [http://dx.doi.org/10.1016/S0034-4257\(00\)00147-4](http://dx.doi.org/10.1016/S0034-4257(00)00147-4).
- Smith, A.M.S., Lentile, L.B., Hudak, A.T., Morgan, P., 2007. Evaluation of linear spectral unmixing and Δ NRB for predicting post-fire recovery in a North American ponderosa pine forest. *Int. J. Remote Sens.* 28, 5159–5166. <http://dx.doi.org/10.1080/01431160701395161>.
- Solans Vila, J.P., Barbosa, P., 2010. Post-fire vegetation regrowth detection in the Deiva Marina region (Liguria-Italy) using Landsat TM and ETM+ data. *Ecol. Model.* 221, 75–84. <http://dx.doi.org/10.1016/j.ecolmodel.2009.03.011>.
- Somers, B., Delaieux, S., Stuckens, J., Verstraeten, W.W., Coppin, P., 2009. A weighted linear spectral mixture analysis approach to address endmember variability in agricultural production systems. *Int. J. Remote Sens.* 30, 139–147. <http://dx.doi.org/10.1080/01431160802304625>.
- Somers, B., Verbesselt, J., Ampe, E.M., Sims, N., Verstraeten, W.W., Coppin, P., 2010. Spectral mixture analysis to monitor defoliation in mixed-aged *Eucalyptus globulus* Labill plantations in southern Australia using Landsat 5-TM and EO-1 Hyperion data. *Int. J. Appl. Earth Obs. Geoinf.* 12, 270–277. <http://dx.doi.org/10.1016/j.jag.2010.03.005>.
- Somers, B., Zortea, M., Plaza, A., Asner, G.P., 2012. Automated extraction of image-based

- endmember bundles for improved spectral unmixing. *IEEE J. Sel. Top. Appl. Earth Obs. Remote Sens.* 5, 396–408. <http://dx.doi.org/10.1109/JSTARS.2011.2181340>.
- Somers, B., Tits, L., Roberts, D., Wetherley, E., 2016. Endmember library approaches to resolve spectral mixing problems in remotely sensed data: potential, challenges, and applications. In: Ruckebush, C. (Ed.), *Data Handling in Science and Technology*. Elsevier, pp. 551–577. <http://dx.doi.org/10.1016/B978-0-444-63638-6.00017-6>.
- Stavros, E.N., Abatzoglou, J.T., McKenzie, D., Larkin, N.K., 2014. Regional projections of the likelihood of very large wildland fires under a changing climate in the contiguous Western United States. *Clim. Chang.* 126, 455–468.
- Stavros, E.N., Tane, Z., Kane, V.R., Veraverbeke, S., McGaughey, R.J., Lutz, J.A., Ramirez, C., Schimel, D., 2016. Unprecedented remote sensing data over king and rim megafires in the Sierra Nevada Mountains of California. *Ecology* 97, 3244. <http://dx.doi.org/10.1002/ecy.1577>.
- Stavros, E.N., Coen, J., Peterson, B., Singh, H., Kennedy, K., Ramirez, C., Schimel, D., 2018. Use of imaging spectroscopy and LIDAR to characterize fuels for fire behavior prediction. *Remote Sens. Appl. Soc. Environ.* <http://dx.doi.org/10.1016/J.RSASE.2018.04.010>.
- Storey, E.A., Stow, D.A., O'Leary, J.F., 2016. Assessing postfire recovery of chamise chaparral using multi-temporal spectral vegetation index trajectories derived from Landsat imagery. *Remote Sens. Environ.* 183, 53–64. <http://dx.doi.org/10.1016/j.rse.2016.05.018>.
- Stuffer, T., Kaufmann, C., Hofer, S., Förster, K.P., Schreier, G., Mueller, A., Eckardt, A., Bach, H., Penné, B., Benz, U., Haydn, R., 2007. The EnMAP hyperspectral imager—an advanced optical payload for future applications in earth observation programmes. *Acta Astronaut.* 61, 115–120. <http://dx.doi.org/10.1016/j.actaastro.2007.01.033>.
- Tane, Z., Roberts, D., Veraverbeke, S., Casas, Á., Ramirez, C., Ustin, S., 2018. Evaluating endmember and band selection techniques for multiple endmember spectral mixture analysis using post-fire imaging spectroscopy. *Remote Sens.* 10, 389. <http://dx.doi.org/10.3390/rs10030389>.
- Thenkabail, P.S., Smith, R.B., De Pauw, E., 2002. Evaluation of narrowband and broadband vegetation indices for determining optimal hyperspectral wavebands for agricultural crop characterization. *Photogramm. Eng. Remote. Sens.* 68, 607–621.
- Thompson, D.R., Boardman, J.W., Eastwood, M.L., Green, R.O., 2017. A large airborne survey of Earth's visible-infrared spectral dimensionality. *Opt. Express* 25, 9186. <http://dx.doi.org/10.1364/OE.25.009186>.
- Tobin, D.C., Revercomb, H.E., Knutson, R.O., Lesht, B.M., Strow, L.L., Hannon, S.E., Feltz, W.F., Moy, L.A., Fetzer, E.J., Cress, T.S., 2006. Atmospheric radiation measurement site atmospheric state best estimates for atmospheric infrared sounder temperature and water vapor retrieval validation. *J. Geophys. Res.* 111, D09S14. <http://dx.doi.org/10.1029/2005JD006103>.
- Trombetti, M., Riaño, D., Rubio, M.A., Cheng, Y.B., Ustin, S.L., 2008. Multi-temporal vegetation canopy water content retrieval and interpretation using artificial neural networks for the continental USA. *Remote Sens. Environ.* 112, 203–215. <http://dx.doi.org/10.1016/J.RSE.2007.04.013>.
- Tucker, C.J., 1980. Remote sensing of leaf water content in the near infrared. *Remote Sens. Environ.* 10, 23–32. [http://dx.doi.org/10.1016/0034-4257\(80\)90096-6](http://dx.doi.org/10.1016/0034-4257(80)90096-6).
- Turetsky, M.R., Kane, E.S., Harden, J.W., Ottmar, R.D., Manies, K.L., Hoy, E., Kasischke, E.S., 2011. Recent acceleration of biomass burning and carbon losses in Alaskan forests and peatlands. *Nat. Geosci.* 4, 27–31. <http://dx.doi.org/10.1038/ngeo1027>.
- Ullah, S., Schlerf, M., Skidmore, A.K., Hecker, C., 2012. Identifying plant species using mid-wave infrared (2.5–6 μm) and thermal infrared (8–14 μm) emissivity spectra. *Remote Sens. Environ.* 118, 95–102. <http://dx.doi.org/10.1016/j.rse.2011.11.008>.
- Ustin, S.L., Roberts, D.A., Pinzón, J., Jacquemoud, S., Gardner, M., Scheer, G., Castañeda, C.M., Palacios-Orueta, A., 1998. Estimating canopy water content of chaparral shrubs using optical methods. *Remote Sens. Environ.* 65, 280–291. [http://dx.doi.org/10.1016/S0034-4257\(98\)00038-8](http://dx.doi.org/10.1016/S0034-4257(98)00038-8).
- van der Werf, G.R., Randerson, J.T., Giglio, L., van Leeuwen, T.T., Chen, Y., Rogers, B.M., Mu, M., van Marle, M.J.E., Morton, D.C., Collatz, G.J., Yokelson, R.J., Kasibhatla, P.S., 2017. Global fire emissions estimates during 1997–2016. *Earth Syst. Sci. Data* 9, 697–720. <http://dx.doi.org/10.5194/essd-9-697-2017>.
- van Leeuwen, W.J.D., Casady, G.M., Neary, D.G., Bautista, S., Alloza, J.A., Carmel, Y., Wittenberg, L., Malkinson, D., Orr, B.J., 2010. Monitoring post-wildfire vegetation response with remotely sensed time-series data in Spain, USA and Israel. *Int. J. Wildland Fire* 19, 75. <http://dx.doi.org/10.1071/WF08078>.
- van Wageningen, J.W., Root, R.R., Key, C.H., 2004. Comparison of AVIRIS and Landsat ETM+ detection capabilities for burn severity. *Remote Sens. Environ.* 92, 397–408. <http://dx.doi.org/10.1016/j.rse.2003.12.015>.
- Varga, T.A., Asner, G.P., 2008. Hyperspectral and LiDAR remote sensing of fire fuels in Hawaii volcanoes National Park. *Ecol. Appl.* 18, 613–623. <http://dx.doi.org/10.1890/07-1280.1>.
- Veraverbeke, S., Hook, S.J., 2013. Evaluating spectral indices and spectral mixture analysis for assessing fire severity, combustion completeness and carbon emissions. *Int. J. Wildland Fire* 22, 707. <http://dx.doi.org/10.1071/WF12168>.
- Veraverbeke, S., Lhermitte, S., Verstraeten, W.W., Goossens, R., 2010. The temporal dimension of differenced normalized burn ratio (dNBR) fire/burn severity studies: the case of the large 2007 Peloponnese wildfires in Greece. *Remote Sens. Environ.* 114, 2548–2563. <http://dx.doi.org/10.1016/j.rse.2010.05.029>.
- Veraverbeke, S., Gitas, I., Katagis, T., Polychronaki, A., Somers, B., Goossens, R., 2012a. Assessing post-fire vegetation recovery using red–near infrared vegetation indices: accounting for background and vegetation variability. *ISPRS J. Photogramm. Remote Sens.* 68, 28–39. <http://dx.doi.org/10.1016/j.isprsjprs.2011.12.007>.
- Veraverbeke, S., Somers, B., Gitas, I., Katagis, T., Polychronaki, A., Goossens, R., 2012b. Spectral mixture analysis to assess post-fire vegetation regeneration using Landsat thematic mapper imagery: accounting for soil brightness variation. *Int. J. Appl. Earth Obs. Geoinf.* 14, 1–11. <http://dx.doi.org/10.1016/j.jag.2011.08.004>.
- Veraverbeke, S., Stavros, E.N., Hook, S.J., 2014. Assessing fire severity using imaging spectroscopy data from the airborne visible/infrared imaging spectrometer (AVIRIS) and comparison with multispectral capabilities. *Remote Sens. Environ.* 154, 153–163. <http://dx.doi.org/10.1016/j.rse.2014.08.019>.
- Veraverbeke, S., Rogers, B.M., Randerson, J.T., 2015. Daily burned area and carbon emissions from boreal fires in Alaska. *Biogeosciences* 12, 3579–3601. <http://dx.doi.org/10.5194/bg-12-3579-2015>.
- Veraverbeke, S., Rogers, B.M., Goulden, M.L., Jandt, R.R., Miller, C.E., Wiggins, E.B., Randerson, J.T., 2017. Lightning as a major driver of recent large fire years in North American boreal forests. *Nat. Clim. Chang.* 7, 529–534. <http://dx.doi.org/10.1038/NCLIMATE3329>.
- Verbesselt, J., Fleck, S., Coppin, P., 2002. Estimation of fuel moisture content towards fire risk assessment: a review. In: *Proc. 6th Int. Conf. For. Fire Res.*, pp. 1–11.
- Vodacek, A., Kremens, R.L., Fordham, A.J., Vangorden, S.C., Luisi, D., Schott, J.R., Latham, D.J., 2002. Remote optical detection of biomass burning using a potassium emission signature. *Int. J. Remote Sens.* 23, 2721–2726. <http://dx.doi.org/10.1080/01431160110109633>.
- Walker, X.J., Rogers, B.M., Baltzer, J.L., Cumming, S.G., Day, N.J., Goetz, S., Johnstone, J.F., Schuur, E.A.G., Turetsky, M.R., Mack, M.C., 2018. Cross-scale controls on carbon emissions from boreal forest mega-fires. *Glob. Chang. Biol.* <http://dx.doi.org/10.1111/gcb.14287>.
- Westerling, A.L., 2006. Warming and earlier spring increase western US forest wildfire activity. *Science* 80, 313. <http://dx.doi.org/10.1126/science.1128834>.
- Whitburn, S., Van Damme, M., Kaiser, J.W., van der Werf, G.R., Turquet, S., Hurtmans, D., Clarisse, L., Clerbaux, C., Coheur, P.-F., 2015. Ammonia emissions in tropical biomass burning regions: comparison between satellite-derived emissions and bottom-up fire inventories. *Atmos. Environ.* 121, 42–54. <http://dx.doi.org/10.1016/j.atmosenv.2015.03.015>.
- Wooster, M.J., Roberts, G., Perry, G.L.W., Kaufman, Y.J., 2005. Retrieval of biomass combustion rates and totals from fire radiative power observations: FRP derivation and calibration relationships between biomass consumption and fire radiative energy release. *J. Geophys. Res.* 110, D24311. <http://dx.doi.org/10.1029/2005JD006318>.
- Yebra, M., Dennison, P.E., Chuvieco, E., Riaño, D., Zylstra, P., Hunt, E.R., Danson, F.M., Qi, Y., Jurdao, S., 2013. A global review of remote sensing of live fuel moisture content for fire danger assessment: moving towards operational products. *Remote Sens. Environ.* 136, 455–468. <http://dx.doi.org/10.1016/j.rse.2013.05.029>.
- Yebra, M., Quan, X., Riaño, D., Rozas Larraondo, P., van Dijk, A.I.J.M., Cary, G.J., 2018. A fuel moisture content and flammability monitoring methodology for continental Australia based on optical remote sensing. *Remote Sens. Environ.* 212, 260–272. <http://dx.doi.org/10.1016/J.RSE.2018.04.053>.
- Yokelson, R.J., Susott, R., Ward, D.E., Reardon, J., Griffith, D.W.T., 1997. Emissions from smoldering combustion of biomass measured by open-path Fourier transform infrared spectroscopy. *J. Geophys. Res. Atmos.* 102, 18865–18877. <http://dx.doi.org/10.1029/97JD00852>.
- Yu, B., Chen, F., Li, B., Wang, L., Wu, M., 2017. Fire risk prediction using remote sensed products: a case of Cambodia. *Photogramm. Eng. Remote. Sens.* 83, 19–25. <http://dx.doi.org/10.14358/PERS.83.1.19>.
- Zhao, F., Meng, R., Huang, C., Zhao, M., Zhao, F., Gong, P., Yu, L., Zhu, Z., 2016. Long-term post-disturbance forest recovery in the greater yellowstone ecosystem analyzed using Landsat time series stack. *Remote Sens.* 8, 898. <http://dx.doi.org/10.3390/rs8110898>.
- Zhukov, B., Lorenz, E., Oertel, D., Wooster, M., Roberts, G., 2006. Spaceborne detection and characterization of fires during the bi-spectral infrared detection (BIRD) experimental small satellite mission (2001–2004). *Remote Sens. Environ.* 100, 29–51. <http://dx.doi.org/10.1016/j.rse.2005.09.019>.